frontiers | Frontiers in Cell and Developmental Biology

TYPE Original Research
PUBLISHED 04 January 2023
DOI 10.3389/fcell.2022.1043259

OPEN ACCESS

EDITED BY
Ramani Ramchandran,
Medical College of Wisconsin,
United States

REVIEWED BY
Jay Trivedi,
Rhode Island Hospital, United States
Lei Zhao,
University of Wisconsin-Madison,
United States

*CORRESPONDENCE
Shigeru Miyaki,
miyaki@hiroshima-u.ac.jp

†These authors have contributed equally to this work and share first authorship

SPECIALTY SECTION
This article was submitted to Molecular and Cellular Pathology, a section of the journal Frontiers in Cell and Developmental Biology

RECEIVED 13 September 2022
ACCEPTED 13 December 2022
PUBLISHED 04 January 2023

CITATION
Fujiwara Y, Ding C, Sanada Y, Yimiti D, Ishikawa M, Nakasa T, Kamei N, Imaizumi K, Lotz MK, Akimoto T, Miyaki S and Adachi N (2023), miR-23a/b clusters are not essential for the pathogenesis of osteoarthritis in mouse aging and post-traumatic models.
Front. Cell Dev. Biol. 10:1043259.
doi: 10.3389/fcell.2022.1043259

miR-23a/b clusters are not essential for the pathogenesis of osteoarthritis in mouse aging and post-traumatic models

Yusuke Fujiwara[1†], Chenyang Ding[1†], Yohei Sanada[1,2], Dilimulati Yimiti[1], Masakazu Ishikawa[1,3], Tomoyuki Nakasa[1,2], Naosuke Kamei[1], Kazunori Imaizumi[4], Martin K. Lotz[5], Takayuki Akimoto[6], Shigeru Miyaki[1,2*] and Nobuo Adachi[1]

[1]Department of Orthopaedic Surgery, Graduate School of Biomedical & Health Sciences, Hiroshima University, Hiroshima, Japan, [2]Medical Center for Translational and Clinical Research, Hiroshima University Hospital, Hiroshima, Japan, [3]Department of Artificial Joints and Biomaterials, Graduate School of Biomedical and Health Sciences, Hiroshima University, Hiroshima, Japan, [4]Department of Biochemistry, Graduate School of Biomedical and Health Sciences, Hiroshima University, Hiroshima, Japan, [5]Department of Molecular Medicine, Scripps Research, La Jolla, CA, United States, [6]Faculty of Sport Sciences, Waseda University, Tokorozawa, Japan

Osteoarthritis (OA), the most prevalent aging-related joint disease, is characterized by insufficient extracellular matrix synthesis and articular cartilage degradation and is caused by various risk factors including aging and traumatic injury. Most microRNAs (miRNAs) have been associated with pathogenesis of osteoarthritis (OA) using *in vitro* models. However, the role of many miRNAs in skeletal development and OA pathogenesis is uncharacterized *in vivo* using genetically modified mice. Here, we focused on miR-23–27–24 clusters. There are two paralogous miR-23–27–24 clusters: miR-23a-27a-24–2 (miR-23a cluster) and miR-23b-27b-24–1 (miR-23b cluster). Each miR-23a/b, miR-24, and miR-27a/b is thought to function coordinately and complementary to each other, and the role of each miR-23a/b, miR-24, and miR-27a/b in OA pathogenesis is still controversial. MiR-23a/b clusters are highly expressed in chondrocytes and the present study examined their role in OA. We analyzed miRNA expression in chondrocytes and investigated cartilage-specific miR-23a/b clusters knockout (Col2a1-Cre; miR-23a/b*flox/flox*: Cart-miR-23clus KO) mice and global miR-23a/b clusters knockout (CAG-Cre; miR-23a/b*flox/flox*: Glob-miR-23clus KO) mice. Knees of Cart- and Glob-miR-23a/b clusters KO mice were evaluated by histological grading systems for knee joint tissues using aging model (12 and/or 18 month-old) and surgically-induced OA model. miR-23a/b clusters were among the most highly expressed miRNAs in chondrocytes. Skeletal development of Cart- and Glob-miR-23clus KO mice was grossly normal although Glob-miR-23clus KO had reduced body weight, adipose tissue and bone density. In the aging model and surgically-induced OA model, Cart- and Glob-miR-23clus KO mice exhibited mild OA-like changes such as proteoglycan loss and cartilage fibrillation. However, the histological scores were not significantly different in terms of the severity of OA in Cart- and Glob-miR-23clus KO mice compared with control mice. Together, miR-23a/b

clusters, composed of miR-23a/b, miR-24, miR-27a/b do not significantly contribute to OA pathogenesis.

KEYWORDS

osteoarthritis, microRNA, cartilage, genetically modified mice, mouse model, bone, aging

1 Introduction

Osteoarthritis (OA) is the most common musculoskeletal disorder caused by risk factors including aging, traumatic injury, and obesity. However, the pathogenesis of OA has not been characterized completely, so currently, there are limited treatment options available for OA prevention or disease modification. Although OA has been considered a disease of cartilage degradation, a recent study indicated that OA is a systemic disease or a whole joint disease accompanied by changes of joint tissues such as subchondral bone (ScB) sclerosis, meniscus degeneration and synovial inflammation (Loeser et al., 2012; Cicuttini and Wluka, 2014; June et al., 2016).

MicroRNAs (miRNAs) are a class of non-coding RNAs involved in fundamental mammalian homeostasis and various diseases through regulating post-transcriptional regulation (Bartel, 2018). It has been reported that various miRNAs regulate chondrocyte homeostasis and inflammatory signaling cascade which are associated with OA pathogenesis (Endisha et al., 2018). Among them, miR-140, which is highly and specifically expressed in cartilage, regulates skeletal development and cartilage homeostasis, and is involved in OA development (Miyaki et al., 2009; Miyaki et al., 2010; Nakamura et al., 2011). Although several miRNAs, such as miR-140 and miR-455, demonstrate the potential to be OA regulatory factors and attractive therapeutical options (Miyaki et al., 2009; Miyaki et al., 2010; Wang et al., 2017; Huang et al., 2019; Duan et al., 2020; Ito et al., 2021), almost all of the studies are analyses by cultured chondrocytes and knee injection with mimic and antioligo for miRNA so far. However, their effects are transient and limited, especially in skeletal development and aging models. Thus, the approaches using genetically modified mice with gain- and loss-of-function model have an advantage in understanding the functions of miRNAs on skeletal and OA development. miR-23a/b clusters, composed of miR-23a–27a–24–2 (miR-23a cluster) and miR-23b–27b–24–1 (miR-23b cluster) are two paralogous miRNA that are located on chromosomes 8 and 13, respectively, in the mouse genome and on chromosomes 19 and 9, respectively, in the human genome. The miRNAs in each of the two clusters of interest are 100% homologous between human and mouse. Each individual miRNA (miR-23a, miR-23b, miR-24, miR-27a, and miR-27b) is finally processed from each cluster for the display of their function as matured miRNAs. Previous reports indicate that among miR-23a/b clusters, miR-23a, miR-24, and miR-27b have a role in maintaining articular cartilage integrity (Akhtar et al., 2010; Philipot et al., 2014; Hu et al., 2017; Zhou et al., 2017; Xu et al., 2018; Lv et al., 2020; Xu et al., 2021). MiR-27, similar to miR-140, is downregulated in patients with OA (Akhtar et al., 2010; Zhou et al., 2017; Xu et al., 2018). On the other hand, miR-23a and miR-23b have been reported to contribute to OA progression (Kang et al., 2016; Guo et al., 2018; Zhao et al., 2019). Non-etheless, these reports have come from cultured chondrocytes with single miRNA mimic or inhibitor such as miR-23a. Each miR-23a/b, miR-24, and miR-27a/b is thought to function coordinately and complementary to each other because they are existing as clusters. Thus, the role of each miRNA that composes miR-23a/b clusters is still controversial in OA pathogenesis. Furthermore, recently, not only cellular miRNAs but also exosomal miRNAs in extracellular vesicles (EVs) such as exosomes have attracted attention for their relation to the pathogenesis, as diagnostic markers, and in the treatment of OA (Miyaki and Lotz, 2018; Mihanfar et al., 2020). The exosomal miR-23a, miR-23b, miR-24, and miR-27b in plasma have been shown to have the potential for development of diagnosis, pathogenesis, and treatments of various diseases including arthritis (Castro-Villegas et al., 2015; Liu et al., 2019; Garavelli et al., 2020; Castanheira et al., 2021). Thus, the role of miR-23a/b clusters in OA pathogenesis firstly requires elucidation by a loss-of-function approach of miR-23a/b clusters using mouse model.

The purpose of the present study is to determine the role of miR-23a/b clusters in OA pathogenesis using cartilage-specific- and global-miR-23a/b clusters deficient mice in two different mouse models of OA, an aging model, and a surgical model.

2 Materials and methods

2.1 Human articular cartilage tissues

Human tissue collection was approved by Human Subjects Committee of Scripps Research or Hiroshima University Hospital. Human articular cartilages from the intact knee joints were procured by tissue banks from 6 donors (mean ± SD age 31.0 ± 15.5 years: female 5, male 1). Cartilages were obtained from 14 patients with OA (mean ± SD age 72.3 ± 7.5 years: female 11, male 3) who were undergoing total knee arthroplasty. All samples were examined by Safranin O staining and graded according to a modified Mankin scale, with a score of < 2 points for normal and a score of > 5 for severe OA. Human chondrocytes were isolated and cultured from articular cartilage as described previously (Maier et al., 1993). The effect size in the

analysis (Normal $n = 6$ vs. OA $n = 14$) was 1.45 with the statistical power of .8 (G power 3.1).

2.2 Nanostring nCounter microRNA analysis

Nanostring nCounter microRNA analysis was performed using RNA from human articular chondrocytes and human articular chondrocytes-derived exosomes as described previously (Furuta et al., 2016). Human articular chondrocytes were cultured with Dulbecco's modified Eagle's medium (DMEM)/10% FBS. One day later, the cells were washed with serum-free DMEM and cultured with serum-free DMEM for 48 h. To isolate the exosomes, 2 ml of conditioned medium was collected and centrifuged for 15 min at 2,380G and then further ultracentrifuged for 70 min at 180,000G at 4°C. The exosome were pellets were resuspended in 100 ml of PBS. The exosomes isolated from the same volume of culture mediums and from the same numbers of cells. Small RNAs were purified from exosome of conditioned medium of cultured human articular chondrocytes using the mirVana miRNA Isolation Kit (Thermo Fisher Scientific Life Sciences, Oakwood Village, OH, https://www.thermofisher.com). Purified small RNAs were concentrated using an evaporator. The concentrations and quality of the small RNAs from the same volume of culture mediums for the same numbers of cells were determined by the BioAnalyzer 2,100 (Agilent Technologies, Santa Clara, CA, http://www.agilent.com), and small RNA was used as the input for the nCounter Human miRNA Expression Assay Kit (NanoString Technologies, Seattle, WA, http://www.nanostring.com) according to manufacturer's instruction.

2.3 Animal study

All animal studies were performed according to protocols approved by Institutional Animal Care and Use Committee at Hiroshima University. All mice were housed in temperature-controlled quarters (23°C ± 1°C) with a 12-h light-dark cycle and in groups of two to five per cage (143 mm × 293 mm × H148 mm) and were freely allowed access to food and water.

2.4 Generation of cartilage-specific miR-23a/b clusters KO mice and global miR-23a/b clusters KO mice

Cartilage-specific miR-23a/b clusters KO (Cart-miR23clus KO) mice and Global miR-23a/b clusters KO (Glob-miR23clus KO) mice were generated by crossbreeding the previously described *Col2*Cre-driver mice (*Col2*Cre mice)(Ovchinnikov et al., 2000) or *CAG*Cre-driver mice (*CAG*Cre mice)(Matsumura et al., 2004) and miR-23a/b clusters floxed mice on C57BL6/J background (Oikawa et al., 2018; Lee et al., 2019). The miR-23a/b clusters$^{flox/flox}$ mice were used as Control. To confirm the miR-23a/b clusters deficiency, we performed the genotyping PCR following PCR primer sets (Supplementary Table S1) as previous reported (Oikawa et al., 2018; Lee et al., 2019). In aging study, we measured the body weight during aging, and body length was measured at the end points of the experiment. Knee joints were harvested at 12 months and/or 18 months of age to monitor spontaneous age-related OA. Control and Cart-miR-23clus KO mice ($n = 7$, $n = 7$), and Control and Glob-miR-23clus KO mice ($n = 11$, $n = 13$) at 12 months of age, and Control and Cart-miR-23clus KO mice ($n = 12$, $n = 12$) at 18 months of age were assessed by histological scoring systems. Experimental OA was induced in Control and Cart-miR23clus KO mice at 12 weeks of age by performing medial meniscectomy and transection of the medial collateral ligament (MCL) in the right knees (Kamekura et al., 2005). Mice were sacrificed at 8 weeks (Control: $n = 8$, Cart-miR-23clus KO: $n = 8$) and 12 weeks (Control: $n = 12$, Cart-miR-23clus KO: $n = 11$) after surgery, and the right knee joints were collected for histological analysis. In the present study, a total of 4 wild type (C57BL6/J), 73 Control, 60 Cart-miR23clus KO and 21 Glob-miR23clus KO mice were sacrificed for histopathological assessment and *in vitro* experiments. All experiments were performed using male mice. Sample sizes were chosen based on prior literature using similar methods (Chang et al., 2019). The previous report demonstrated moderate effect size (> 1.7) in aging model (Control mice $n = 8$ vs. KO mice $n = 8$) and moderate effect size (> 1.5) in surgically-induced OA model (Control mice $n = 9$ vs. KO mice $n = 9$). We determined the sample size appropriate to maintain the effect size of 1.5 with statistical power of .8 (G power 3.1) and performed a minimum of $n = 7$. However, we were determined to perform $n = 12$ considering issues such as life span of genetically modified mice and loss of mice due to various causes in aging model of 18 months of age.

2.5 Histopathological assessments

Whole-mount Alcian blue (Sigma-Aldrich, United States) and Alizarin red S (Sigma-Aldrich, United States) staining of skeletons were performed on Control, Cart-miR23clus KO and Glob-miR23clus KO mice at postnatal day 0. All knee joints were embedded intact in paraffin after fixation in 4% paraformaldehyde phosphate buffer solution (PBS) and decalcification in K-CX or EDT-X (FALMA, Japan). Knee joints were sectioned (4.5 μm) in the coronal plane anterior to posterior through the central weight-bearing region of the femorotibial joint. The sections were stained with Safranin O (MUTO PURE CHEMICALS, Tokyo, Japan) and Fast Green (Sigma-Aldrich, United States) and three different sections per

joint were analyzed microscopically. Three different researchers were blinded while performing all manual scorings. Damage to the articular cartilage (maximum of 24 points per knee joint section; 6 points for each quadrant of the tibial/femoral cartilage) was evaluated using the OARSI scoring system (Glasson et al., 2010). Subchondral bone changes, meniscus degradation and the severity of synovitis were evaluated using the right knee joints according to previously described histopathological scoring systems (Krenn et al., 2002; Kwok et al., 2016; Nagira et al., 2020).

2.6 Immunohistochemical analysis

Slides were pretreated with antigen-retrieval reagent (Immunoactive; Matsunami Glass Ind, Osaka, Japan) at 60°C for 16 h, followed by blocking serum for 30 min. Then, sections were immunostained with anti-$P16^{INK4a}$ antibody (abcam, ab54210, 0.1 μg/ml), anti-ADAMTS5 antibody (GeneTex, GTX100332, 10 μg/ml) and anti-MMP13 antibody (ThermoFisher Scientific, MA5-14328, 20 μg/ml) diluted in Can Get Signal immunostaining solution (TOYOBO, Tokyo, Japan) using Vectastain ABC-AP alkaline phosphatase kit and AP substrate kit (Vector Laboratories, Burlingame, CA, United States) according to the manufacturers' instructions. For type II and type X collagen staining, slides were pretreated with antigen retrieval reagent (Proteinase K, Dako, CA, United States) at room temperature for 10 min and blocking serum for 30 min. Then, sections were immunostained with anti-type II collagen antibody (DSHB, CIIC1, 6 μg/ml) and anti-type X collagen antibody (DSHB, X-AC9, 5 μg/ml) diluted in PBS using Vectastain Elite ABC-HRP kit and DAB substrate kit. All stainings and evaluations were performed using $n = 5$ each group.

2.7 Mouse chondrocytes isolation and culture

Articular cartilage from the femoral heads of mice at 3 weeks of age was taken, and chondrocytes were isolated by digestion with 3.5 mg/ml collagenase Type 2 (Worthington, Lakewood, NJ, United States) in Dulbecco's modified Eagle's medium (DMEM) (FUJIFILM Wako, Osaka, Japan) for 1.5 h at 37°C. Isolated chondrocytes were cultured in DMEM with 10% fetal bovine serum. Experiments were carried out at passage 1. Chondrocytes were treated with or without IL-1β (1 ng/ml; Pepro-Tech, Rocky Hill, NJ, United States) for 24 h.

2.8 Quantitative real-time PCR

Total RNA was extracted from various tissues and cultured chondrocytes using Isogen reagent (Nippon gene, Tokyo, Japan) and RNA purification kit (Direct-zol RNA microprep, Zymo Research, California, United States). Small RNA from serum was extracted using Maxwell RSC miRNA Plasma and Serum kit (Promega, Wisconsin, United States). Complementary DNA (cDNA) was synthesized with a Reverse Transcription system (iScript supermix, BioRad, California, United States) according to the manufacturer's protocol. Quantitative polymerase chain reaction (PCR) was performed with the TaqMan Gene Expression Assay probes (Supplementary Table S2) (Thermo Fisher Scientific, Massachusetts, United States). *Gapdh* and U6 snRNA were used as the internal controls to normalize the sample differences. Relative expression was calculated using the ΔΔCt values, and results were expressed as $2^{-\Delta\Delta Ct}$.

2.9 Glycosaminoglycan release assay

Femoral head cartilages (femoral cap: Control $n = 8$, Cart-miR-23clus KO $n = 7$) were harvested from 3-week-old Control and Cart-miR-23a/b clusters KO mice and weighed. The amount of the released glycosaminoglycan into medium was measured using the Blyscan Glycosaminoglycan assay kit (Biocolor, United Kingdom) as previously described (Ishitobi et al., 2018). Size variance between femoral caps was normalized by their weight.

2.10 Immunoblotting analysis

Protein was extracted from cultured chondrocytes using M-PER™ protein extraction reagent (Thermo Fisher Scientific) with protease inhibitor cocktail set I (FUJIFILM Wako) and phosphatase inhibitor cocktail I (abcam). Total protein (20 μg–30 μg) was separated by SDS/PAGE (10%), and electrically transferred onto PVDF membranes (BioRad). After blocking with 5% skim milk in TBST, the membranes were incubated with primary antibodies and then incubated with secondary antibodies. The signal was detected with chemiluminescent of enhanced immunostar SD (FUJIFILM Wako). The quantifications of immunoblotting were performed using ImageJ (version 1.53o). Antibodies used in immunoblotting are listed in Supplementary Table S3. All immunoblottings were performed using $n = 5$ each group.

2.11 DEXA analysis

The skin and muscles were removed from the hind limbs which were fixed in 4% paraformaldehyde phosphate buffer solution (PBS) for 48 h at 4°C. Bone mineral density (BMD) in femur bone ($n = 7$ each group: Control and Glob-miR-23clus KO mice at 12 months of age) was measured using dual-energy X-ray absorptiometry (DEXA) densitometry (Aloka DCS-600EX, Aloka Co., Tokyo, Japan). Bone density measurements

of left femur were taken from sixteen consecutive images with a scan pitch of 2 mm by DEXA scan from the distal femur.

2.12 TUNEL staining

TUNEL staining was completed using an *in-situ* detection kit for programmed cell death detection (MEBSTAIN apoptosis TUNEL Kit direct: MBL, United States) according to the manufacturer's instructions. Nuclei were stained by 4′,6-diamidino-2-phenylindole (DAPI). TUNEL staining were performed using $n = 5$ each group.

2.13 Multiomics analysis

Articular chondrocytes from the femoral heads of mice at 3 weeks of age were isolated by digestion with 3.5 mg/ml collagenase Type 2 (Worthington, Lakewood, NJ, United States) in DMEM (FUJIFILM Wako, Osaka, Japan) for 1.5 h at 37°C. Isolated chondrocytes were cultured in DMEM with 10% fetal bovine serum. Primary chondrocytes were harvested from dishes after reaching confluency and seeded in 6-well plates at 5×10^5 cells per well. Total RNA and protein of Control and, Cart-miR-23a/b KO chondrocytes were extracted and underwent Multiomics (RNA-sequencing and DIA proteome) analysis at Kazusa Genome Technologies (Kisarazu, Japan). Quantitative analysis of proteomes was performed by the data-independent acquisition (DIA) proteome analysis using Q-Exactive™ HF-X (Thermo Fisher Scientific) as described previously (Kawashima et al., 2019). The mass spectrometry proteomics data that can be accessed have been deposited to the ProteomeXchange Consortium *via* the PRIDE partner repository with the dataset identifier, PXD031868. RNA-seq libraries were prepared using QuantSeq 3′mRNA-Seq Library Prep Kit for Illumina (FWD) (015.384, LEXOGEN). RNA-Seq was carried out using single-end 75 base read sequencing using an Illumina NextSeq500 sequencer. After checking the quality of the reads, it was determined that filtering of low-quality reads was not necessary. The reads were mapped to the mouse reference genome (10 mm) and the expression of the identified genes was normalized by calculation of TPM. The RNA-seq data have been deposited in NCBI's Gene Expression Omnibus and are accessible through GEO Series accession number, GSE197363 (https://www.ncbi.nlm.nih.gov/geo/query/acc.cgi?acc=GSE197363). Differentially expressed genes were extracted and subsequently imported into gene ontology enrichment analysis with Metascape (https://metascape.org) (Zhou et al., 2019).

2.14 Statistical analysis

Actual measurement values of all data are presented as mean ± standard error of mean (SEM) or standard deviation (SD). For comparison between two groups, Welch's *t*-test or Mann-Whitney *U* test was applied. For multiple comparison, *p*-values were corrected with Holm-Sidak method (Graph Pad Prism 9.0). Scoring data in aging OA model and surgically-induced OA model was analyzed for differences between mouse type and time-points using nonparametric Kruskal-Wallis test, then the *post-hoc* Dunn's test or Mann-Whitney *U* test to evaluate individual comparisons. Body weight and bone density were analyzed with two-way ANOVA, then *post hoc* Sidak's test to evaluate individual comparisons. Differences were considered statistically significant at $p < .05$. Sample sizes were chosen based on prior literature using similar methods, reporting moderate effect size, and our previous experiments.

3 Results

3.1 Expression patterns of miR-23a/b clusters in articular cartilage

To characterize the expression profile of miRNAs in normal human articular chondrocytes, we first performed miRNA expression analysis using Nanostring nCounter (Supplementary Table S4). In this analysis, we focused on miR-23a/b clusters which were expressed at higher levels than miR-140 in chondrocytes. The expression of miR-23a/b clusters was observed in various tissues of C57BL/6J mice at 4 weeks of age, wherein they were expressed more abundantly in the lung and articular cartilage (Figure 1A). Among miR-23a/b clusters, especially miR-24 was highly expressed in various tissues including articular cartilage. These results demonstrated that miR-23a/b clusters were expressed in a broad range of tissues but not in cartilage-specific expression pattern. However, the expression levels of miR-23a/b clusters were especially higher in cartilage including intervertebral disc and lung than other tissues. Furthermore, we examined the expression of miR-23a/b clusters in articular chondrocytes from normal and OA cartilage (Figure 1B). The expression of miR-23a, miR-24 and miR-27a was significantly decreased in OA chondrocytes compared with normal chondrocytes consistent with prior findings about miR-140 (Figure 1C). Thus, previous inconsistent reports (Akhtar et al., 2010; Philipot et al., 2014; Hu et al., 2017; Zhou et al., 2017; Xu et al., 2018; Lv et al., 2020; Xu et al., 2021) and our results prompted us to examine the role of miR-23a/b clusters in cartilage development and OA pathogenesis using miR-23a/b clusters-deficient mice. We expected that 23a/b clusters-deficient mice would exhibit abnormal skeletal development and altered onset or severity of OA.

3.2 Cartilage-specific miR-23a/b clusters loss-of-function model

The expression pattern of miR-23a/b clusters was ubiquitous. To examine the role of miR-23a/b clusters in cartilage, we

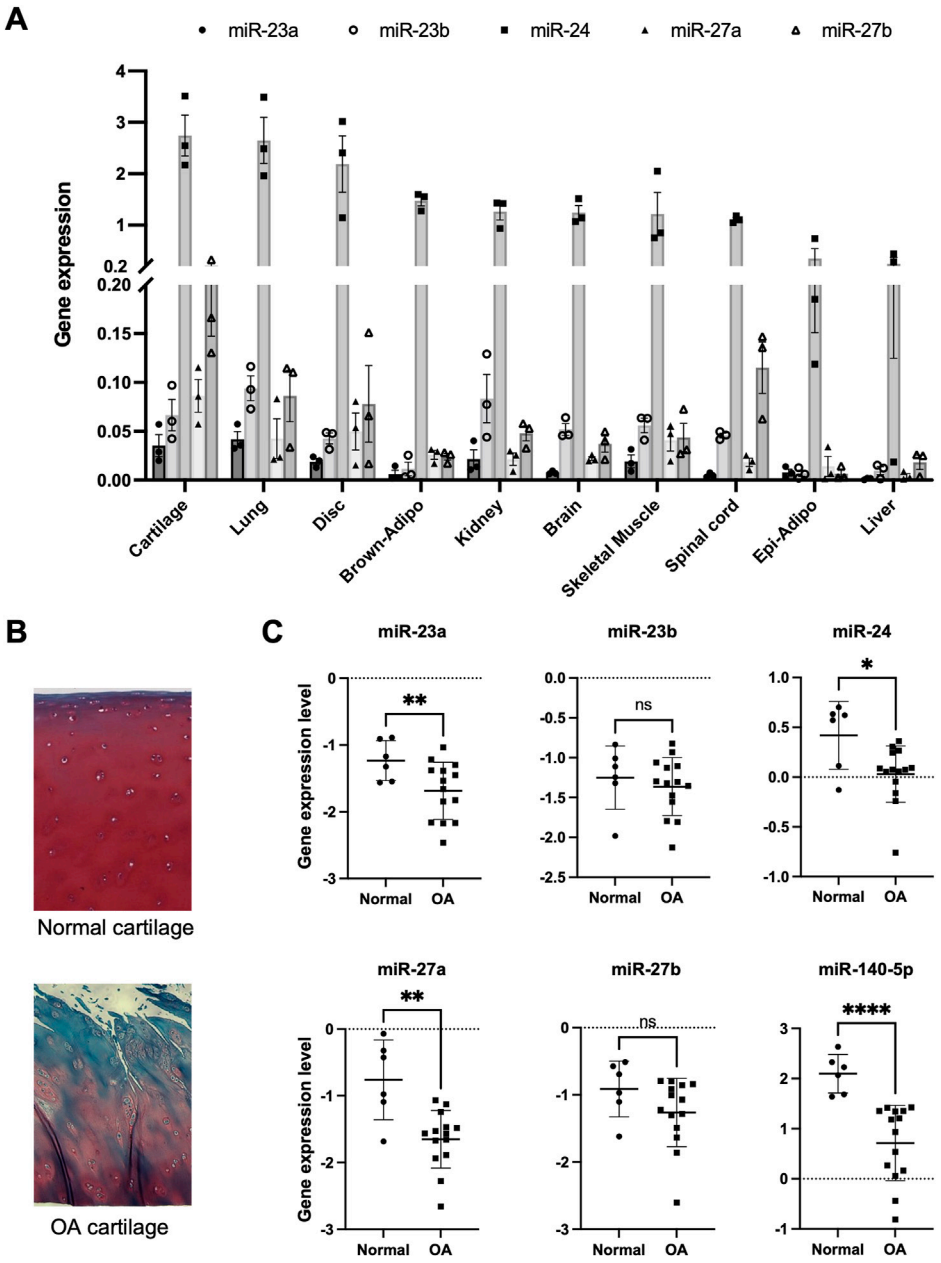

FIGURE 1
Expression pattern of miR-23a/b clusters in various tissues and osteoarthritis cartilage. **(A)** miR-23a/b clusters were expressed in various tissues (Cartilage: articular cartilage, Lung, Disc: intervertebral disc, Brown-Adipo: brown adipose tissue, Kidney, Brain, Skeletal muscle, Spinal cord, Epi-Adipo: epididymal adipose tissue, and Liver: n = 3 each tissue) of C57BL6/J mice at 4 weeks of age by real-time PCR analysis. **(B)** Normal human cartilage and OA cartilage for Isolation of Articular chondrocytes. Representative histological image with Safranin-O staining. **(C)** The expression of miR-23a/b clusters and miR-140 in articular chondrocytes from human normal cartilage (n = 6) and OA cartilage (n = 14). All data are represented as mean ± SEM. Comparison of mean values was performed by Welch's t-test; *p < .05, **p < .01, ****p < .0001 *versus* normal chondrocytes. n. s: non-significant difference.

performed experiments through a cartilage-specific loss-of-function approach using Cart-miR-23clus KO mice. Cart-miR-23clus KO mice were generated by crossing miR-23a/b clusters floxed mice (Lee et al., 2019) with *Col2*-Cre Tg mice (Ovchinnikov et al., 2000). The expression levels of miR-23a cluster (miR-23a–27a–24–2) and miR-23b cluster (miR-23b–27b–24–1) were decreased specifically in cartilage and chondrocytes of Cart-miR-23clus KO mice compared with Control mice (Supplementary Figures S1A, B). However, Cart-miR-23clus KO mice postnatally showed no difference in skeletal

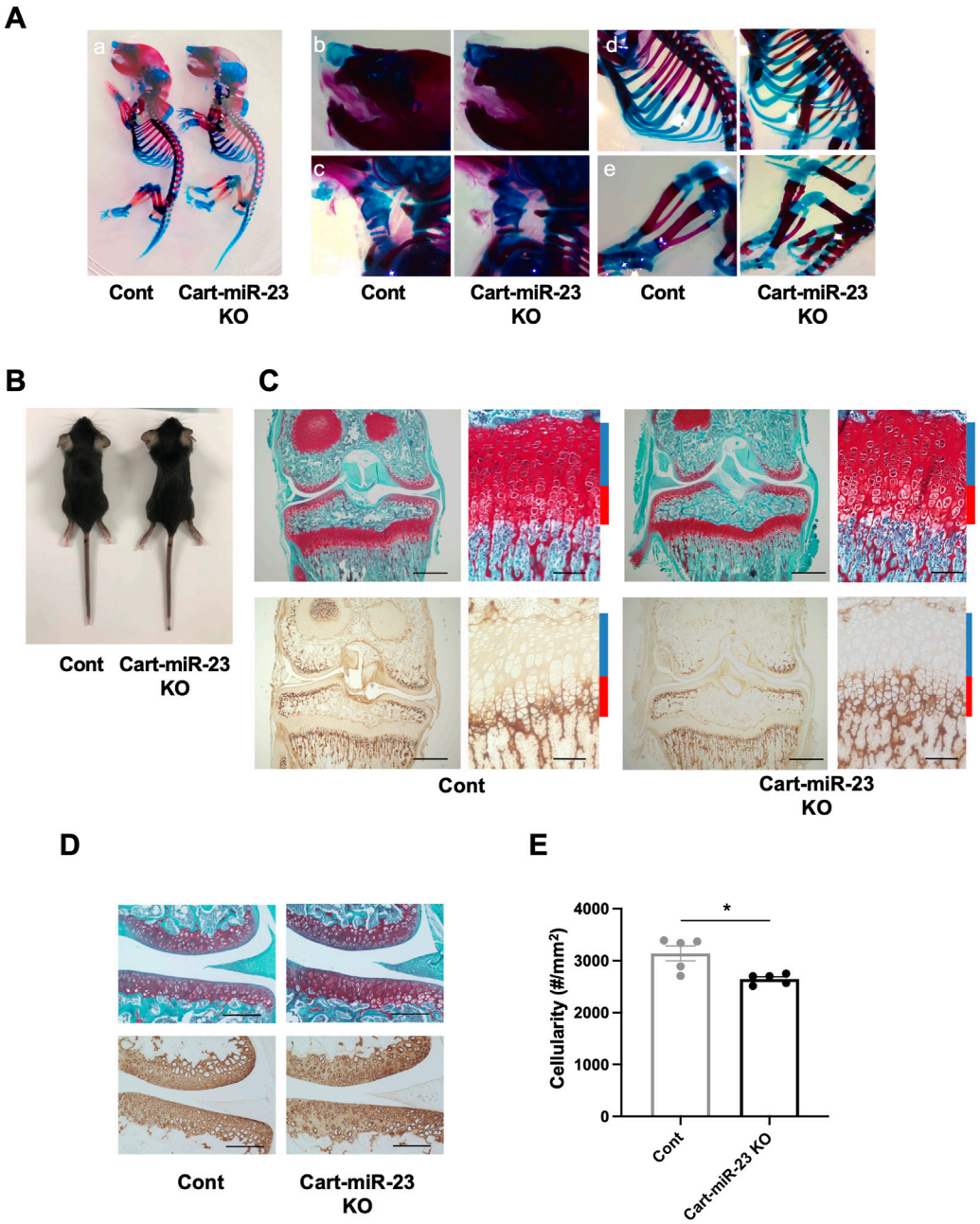

FIGURE 2
Skeletal development in Cart-miR-23clus KO mice. **(A)** Skeletal preparation with Alcian blue/Alizarin red staining of Control and Cart-miR-23clus KO mice in postnatal day 0. **(A)** Whole mount, **(B)** nasal capsule, **(C)** trachea, **(D)** rib cage, **(E)** hind limb. Cart-miR-23clus KO mice exhibited no overt abnormality in skeletal development. **(B)** Appearance of Control and Cart-miR-23clus KO mice at 3 weeks of age. Growth retardation was not observed in Cart-miR-23clus KO mice. **(C)** Safranin O/Fast Green staining and immunohistochemistry (Type X Collagen) in articular cartilage of knee joints and in the tibial growth plate in Control and Cart-miR-23clus KO mice at 3 weeks of age. Scale bars: 500 μm and 100 μm. **(D)** Safranin O/Fast Green staining and immunohistochemistry (Type II Collagen) in articular cartilage of knee joints in Control and Cart-miR-23clus KO mice at 3 weeks of age. Scale bars: 200 μm. **(E)** Cellularity in articular cartilage of Control and Cart-miR-23clus KO mice (n = 5 per group). The data represented as mean ± SEM. Comparison of mean values was performed using Welch's t-test; *p < .05.

development (Figures 2A–E, B). The articular cartilage and growth plate staining with Safranin O, type X Collagen, and type II Collagen, and the structure and shape of the knee joints and their menisci were normal in Cart-miR-23clus KO mice at 3 weeks of age (Figures 2C, D). Although the cellularity of articular cartilage was significantly decreased in Cart-miR-

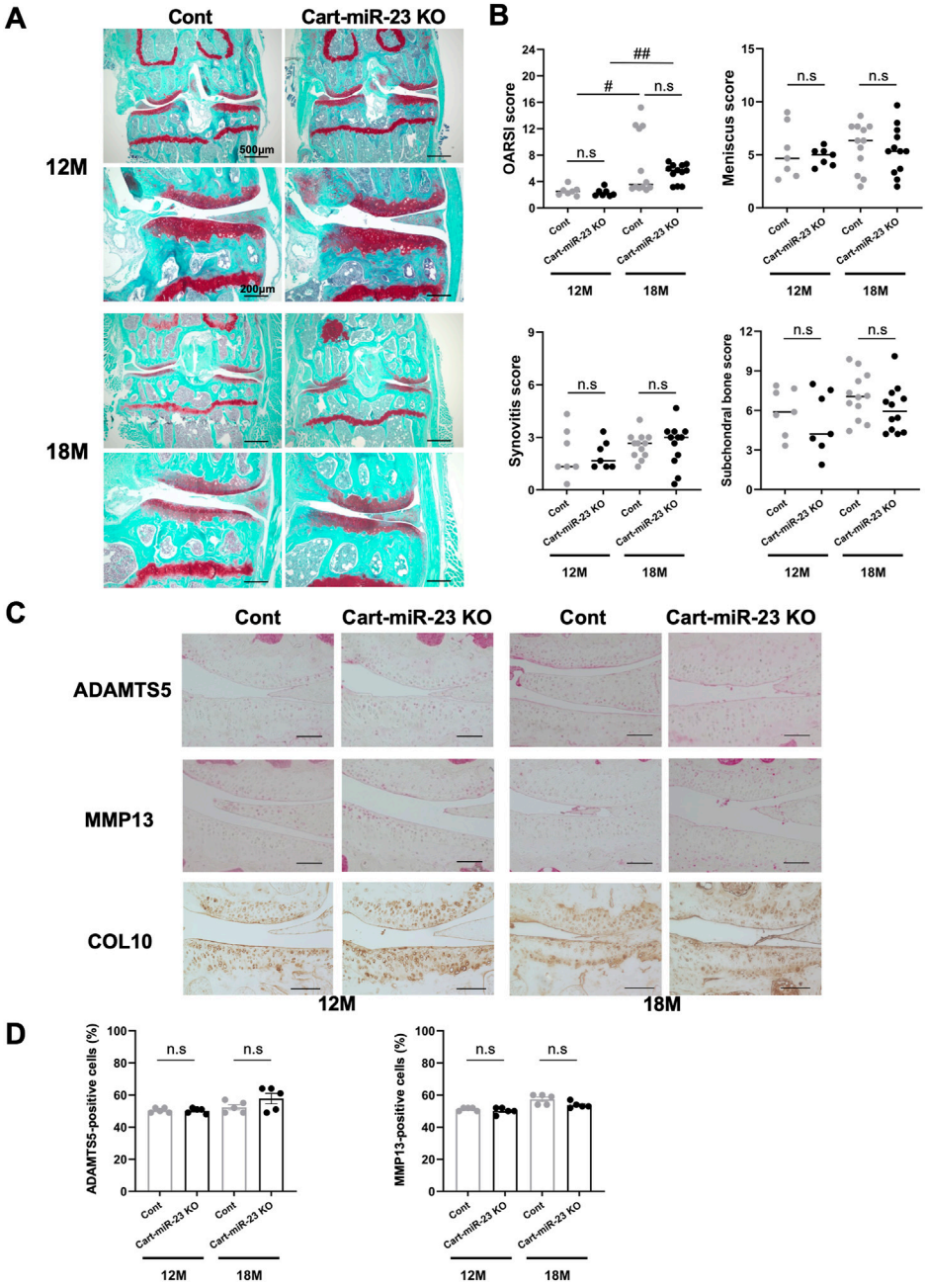

FIGURE 3
Histopathological evaluation of Knee joint tissues in Cart-miR-23clus KO mice with aging. **(A)** Safranin O staining of the knee joints of Control and Cart-miR-23clus KO mice at 12 and 18 months of age. Scale bars: 500 μm and 200 μm. **(B)** The right knee joints of Control and Cart-miR-23clus KO mice at 12 months of age (Control: $n = 7$, Cart-miR-23clus KO: $n = 7$) and 18 months of age (Control: $n = 12$, Cart-miR-23clus KO: $n = 12$) were assessed by OARSI scoring, meniscus scoring, synovitis scoring and ScB scoring system. The data was represented as median. Scoring data was analyzed by Kruskal–Wallis test, the Dunn's multiple comparison test was applied; $^{\#}p < .05$, $^{\#\#}p < .01$. **(C,D)** Knee joints from Control and Cart-miR-23clus KO mice were assessed by immunohistochemistry using anti-ADAMTS5, anti-MMP13, and anti-Type X Collagen antibodies ($n = 5$ per group). Scale bars: 100 μm. The data represented as mean ± SEM. Comparison of mean values was performed using Welch's *t*-test with Holm-Sidak correction for multiple comparison. n. s: non-significant difference.

23clus KO mice compared with Control mice (Figures 2D, E), Cart-miR-23clus KO mice exhibited almost normal skeletal development and maturation.

To determine whether miR-23a/b clusters have role in the pathogenesis of OA, we examined the knee joints of Cart-miR-23clus KO mice in two different mouse models of OA, an aging

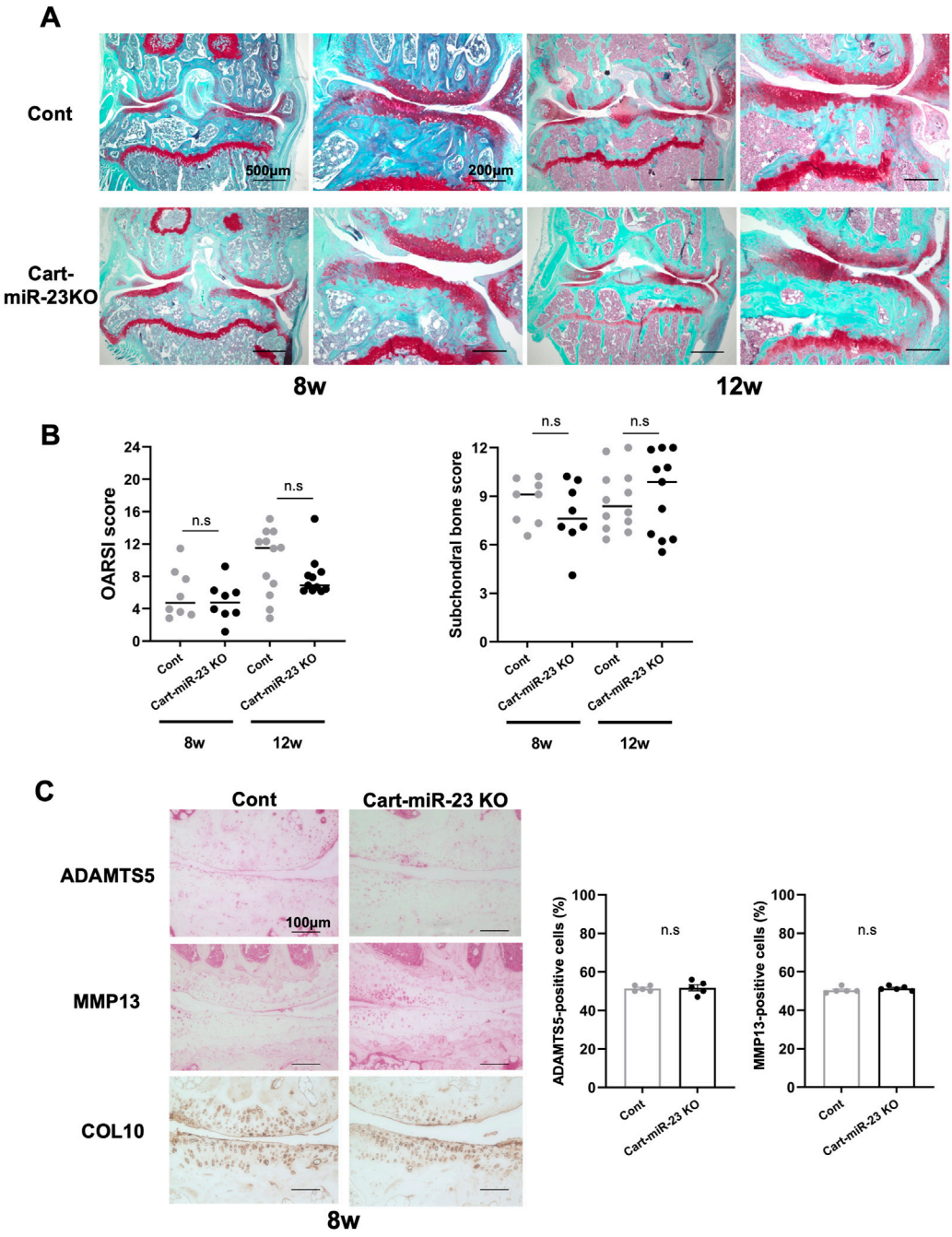

FIGURE 4
Histopathological evaluation of Knee joint tissues of Cart-miR-23clus KO mice in surgically induced OA model. **(A)** Safranin-O staining in the knee joints of Control and Cart-miR-23clus KO mice in surgically induced OA model. Scale bars: 500 μm and 200 μm. **(B)** The right knee joints of Control and Cart-miR-23clus KO mice after 8 weeks (Control: $n = 8$, Cart-miR-23clus KO: $n = 8$) and 12 weeks (Control: $n = 12$, Cart-miR-23clus KO: $n = 11$) of surgery were assessed by OARSI scoring and ScB scoring system. The data was represented as median. Scoring data was analyzed by Kruskal–Wallis test, then Dunn's multiple comparison test was applied. **(C)** Knee joints from Control and Cart-miR-23clus KO mice after 8 weeks of surgery were assessed by immunohistochemistry using anti-ADAMTS5, anti-MMP13, and anti-type X Collagen antibodies ($n = 5$ per group). Scale bars: 100 μm. The data represented as mean ± SEM. Comparison of mean values was performed using Welch's *t*-test. n. s: non-significant difference.

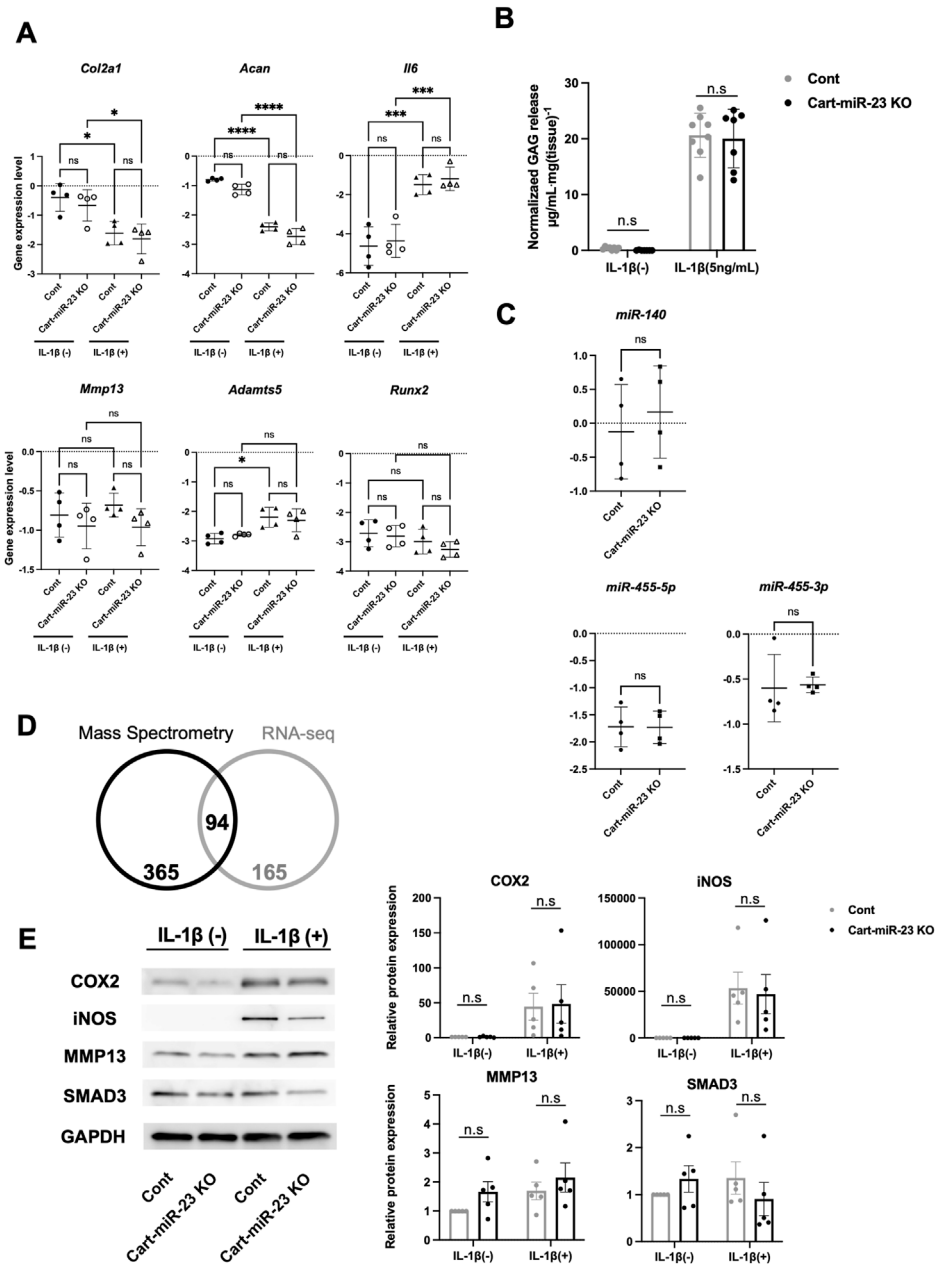

FIGURE 5
Osteoarthritis related markers in the articular chondrocytes of Cart-miR-23a/b KO mice. **(A)** Real-time PCR was performed to assess the OA-related genes expression in articular chondrocytes with or without IL-1β treatment (1 ng/ml for 24 h) from Control and Cart-miR-23clus KO mice (n = 4 each group) at 3 weeks of age. **(B)** Femoral head cartilage explants from Control and Cart-miR-23clus KO mice (Control: n = 8, Cart-miR-23clus KO: n = 7) cultured with or without IL-1β (5 ng/ml) for 72 h. Proteoglycan release into the conditioned medium from articular cartilage was assayed as the concentration of glycosaminoglycan (GAG). **(C)** Expression of cartilage-related miRNAs in Control and Cart-miR-23clus KO articular chondrocytes by real-time PCR (n = 4 each group). **(D)** Venn diagram comparing upregulated proteins and mRNAs (Cart-miR-23clus KO/wild-type mice) in proteome analysis and transcriptome analysis. **(E)** Western blotting of NF-κB-dependent proteins in Control and Cart-miR-23clus KO articular chondrocytes (n = 5 each group) with or without IL-1β treatment. All data represented as mean ± SEM. Comparison of gene expression **(A)**, GAG release **(B)** and protein expression **(E)** were performed using one-way ANOVA Sidak's multiple comparisons test. Comparison of mean values **(C)** was performed using Welch's t-test. *p < .05, **p < .01, ***p < .001, ****p < .0001. n. s: non-significant difference.

model as primary OA, and a surgical model as posttraumatic OA. First, in aged mice, the bodyweight and the body length of Cart-miR-23clus KO mice were similar with that of Control mice at 12 months of age (Control mice: mean ± SD body weight 36.9 g ± 2.8 g and body length 9.7 cm ± .3 cm, Cart-miR-23clus KO mice: 35.5 g ± 2.8 g, 9.6 cm ± .3 cm) and 18 months of age (Control mice: body weight 36.7 g ± 2.5 g and body length 10.2 cm ± .3 cm, Cart-miR-23clus KO mice: 36.8 g ± 5.8 g, 9.8 cm ± .3 cm). Cart-miR-23clus KO mice at 12 months of age exhibited almost normal knee joint tissues including articular cartilage with similar proteoglycan staining, meniscus, synovium, and ScB (Figures 3A,B). At 18 months of age, several Cart-miR-23clus KO mice and Control mice showed reduced Safranin O staining especially in the medial tibial plateau, indicating proteoglycan loss, a roughened articular surface, and fibrillations (Figure 3A). Furthermore, they also showed medial meniscus degeneration, synovitis, and ScB changes with sclerosis in medial tibia (Figure 3A). Although OARSI, meniscus and ScB scores demonstrated more progressive OA-like changes in both mice at 18 months of age than at 12 months of age, there was no significant difference between Cart-miR-23clus KO mice and Control mice at 12 and 18 months of age (Figure 3B). There were no changes in the expression patterns of OA-related markers, ADAMTS5, MMP13, and Type X Collagen between the Control mice and Cart-miR-23clus KO mice (Figures 3C, D).

Next, we investigated surgically-induced OA model mice as posttraumatic OA. Both Cart-miR-23clus KO mice and Control mice exhibited mild OA-like changes with proteoglycan loss after 8 weeks of surgery, and the OARSI and ScB scores were not significantly different (Figures 4A, B). After 12 weeks of surgery, both strains of mice exhibited more severe OA-like changes with partial cartilage defects and osteophytes on the medial tibial plateau (Figures 4A,B). OARSI scores indicated more progressive OA-like changes in both mice at 8 weeks and 12 weeks after surgery. However, there was no significant difference between Cart-miR-23clus KO mice and Control mice (Figure 4B). ADAMTS5 and MMP13 expression in articular cartilage did not change in both strains at 8 weeks after surgery (Figure 4C). These results indicated that deficiency of miR-23a/b clusters in chondrocytes does not affect posttraumatic OA severity.

3.3 Gene expressions in chondrocytes from miR-23clus KO mice

Furthermore, we investigated OA-related genes expression and the responses to IL-1β-treatment in chondrocytes from Cart-miR-23clus KO mice at 3 weeks of age. IL-1β stimulation induced a significant increase in the expression of *Adamts5* and inflammatory *Il6* and a significant decrease in the expression of *Col2a1* and *Acan* in chondrocytes from Control mice and/or Cart-miR-23clus KO mice (Figure 5A). However, there were no significant differences between Control mice and Cart-miR-23clus KO mice (Figure 5A). Furthermore, GAG loss levels from articular cartilage of the Cart-miR-23clus mice were not significantly different from that of the Control mice (Figure 5B). Thus, the responses to IL-1β in Cart-miR-23clus KO chondrocytes were similar with Control chondrocytes. The expression of cartilage-related miRNAs, such as miR-140 and miR-455, had no significant changes between Control and Cart-miR-23clus KO chondrocytes (Figure 5C).

3.4 Target genes of miR-23 a/b clusters

To investigate mRNA and protein level of miR-23a/b clusters target candidates, we performed multiomics analysis using wild-type chondrocytes and Cart-miR-23clus KO chondrocytes. Four hundred and fifty-nine target candidate genes for miR-23a/b clusters (2-fold increase for Cart-miR-23clus KO chondrocytes compared to Control) were identified by proteomics analysis, and 94 genes were commonly upregulated in mRNA and protein level (Figure 5D; Supplementary Table S5). To further investigate the altered biological processes as a result of miR-23a/b clusters-deletion in chondrocytes, gene ontology (GO) analysis was performed. The upregulated genes were involved in biological processes such as cell adhesion, and downregulated genes were involved in ossification (Supplementary Figures S2, S3). Furthermore, although previous reported target genes were not included in the 94 target candidate genes, to validate NF-κB-dependent genes and *Smad3* as target genes of miR-23a/b clusters, we performed Western Blotting analysis using Control and Cart-miR-23clus KO chondrocytes with or without IL-1β treatment. Although the protein levels of COX2, iNOS and MMP13 were upregulated in Control and miR-23clus KO chondrocytes with IL-1β treatment, there were no significant changes in their upregulation in miR-23clus KO chondrocytes compared with Control chondrocytes (Figure 5E). SMAD3 had no significant difference between Control and miR-23clus KO chondrocytes.

3.5 Global miR-23a/b clusters loss-of-function model

Furthermore, investigating the role of miR-23a/b clusters in tissues other than cartilage is also important for the skeletal development and the pathogenesis of OA as whole joint or systemic disease. Exosomal miRNAs, which are miRNAs existing in EVs such as exosomes, recently have attracted increasing attention because of their relation to the pathogenesis of various diseases and as newly mediators of tissue-to-tissue/cell-to-cell communication (Valadi et al., 2007; Mori et al., 2019). Thus, to further define the function of miR-23a/b clusters by global deletion

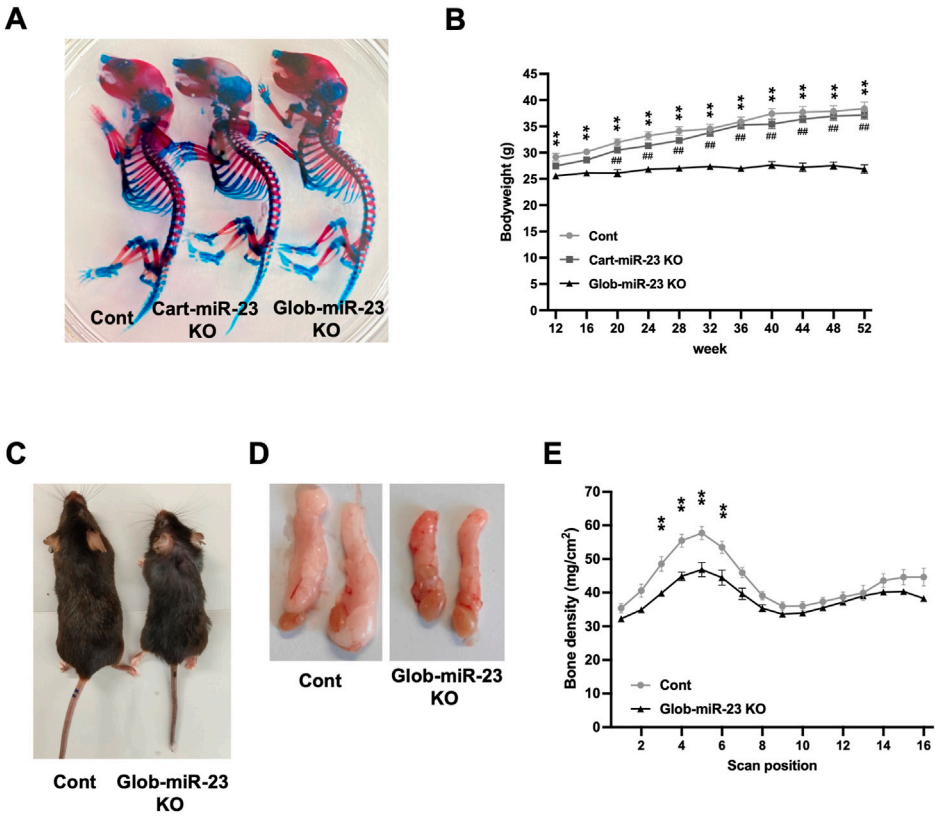

FIGURE 6
Growth retardation and accelerating aging-like phenotype in Glob-miR-23clus KO mice. **(A)** Skeletal preparation with Alcian blue/Alizarin red staining of Control, Cart-miR-23clus KO, and Glob-miR-23clus KO mice at postnatal day 0. **(B)** Bodyweight during aging. Glob-miR-23clus KO mice exhibited growth retardation during aging. Control: n = 11, Cart-miR-23clus KO mice: n = 7, Glob-miR-23clus KO mice: n = 13. **(C,D)** Representative images of whole body and epididymal adipose tissue in Control and Glob-miR-23clus KO mice at 12 months of age. **(E)** Bone mineral density in Control and Glob-miR-23clus KO mice at 12 months of age (n = 7 each group). All data was represented as mean ± SEM. The data **(B,E)** was analyzed by two-way ANOVA; $^{**}p < .01$:Glob-miR-23clus KO vs. Control, $^{\#\#}p < .01$:Glob-miR-23clus KO vs. Cart-miR-23clus KO.

including cellular and exosomal miRNA, we evaluated Glob-miR-23clus KO mice with aging. Glob-miR-23clus KO mice, in which miR-23a/b clusters were deleted under the control of the synthetic CAG promoter, exhibited the downregulation of ubiquitous miR-23a/b clusters expression (Supplementary Figure S4). Exosomal miR-23a/b clusters, miR23a, miR-23b, and miR-24 were undetected in serum of Glob-miR-23clus KO mice. miR-27a and miR-27b were undetected in the serum of Control and Glob-miR-23clus KO mice. Skeletal development in Glob-miR-23clus KO mice at postnatal day 0 appeared grossly normal compared with Control mice (Figure 6A). The bodyweight of Glob-miR-23clus KO mice was significantly lower than Control mice and Cart-miR-23clus KO mice throughout aging until 12 months of age (Figure 6B). Their body size and adipose tissue volume were significantly lower than Control mice at 12 months of age (Figures 6C, D). Furthermore, Glob-miR-23clus KO mice exhibited low bone density (Figure 6E). However, Glob-miR-23clus KO mice did not exhibit knee joints with severe OA-like changes at 12 months of age, each score had no significant difference between Control mice and Glob-miR-23clus KO mice (Figures 7A, B). Although the number of cells positive for $p16^{INK4a}$, a marker of senescent cells, were significantly increased in articular cartilage of Glob-miR-23clus KO mice, TUNEL-positive chondrocytes in superficial and middle layer were decreased in Glob-miR-23clus KO mice (Figures 7C, D). Type X Collagen and ADAMTS5 had no changes between articular cartilage of Control mice and Glob-miR-23clus KO mice (Figures 7E, F). MMP13 was significantly increased in articular cartilage of Glob-miR-23clus KO mice (Figures 7E, F). However, Glob-miR-23clus KO mice also did not exhibit acceleration of OA development.

4 Discussion

In the present study, we determined the role of miR-23a/b clusters, which are highly expressed in cartilage, in the pathogenesis of OA using two OA models in miR-23a/b clusters KO mice. Among miR-23a/b clusters, miR-23a, miR-23b and miR-27b have been suggested to have a role in

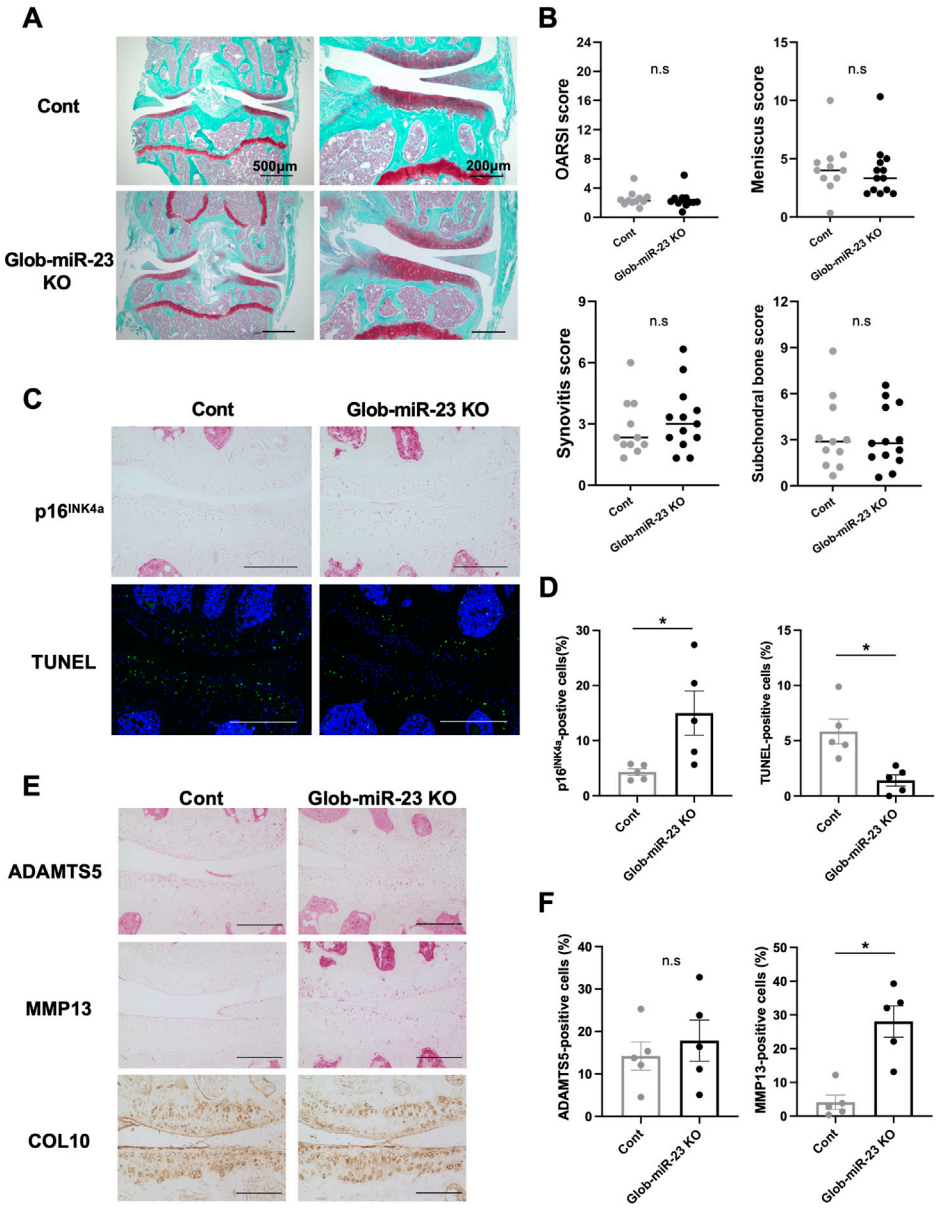

FIGURE 7
Histopathological evaluation of Knee joint tissues in Glob-miR-23clus KO mice with aging. **(A)** Safranin O staining of the knee joints of Control and Glob-miR-23clus KO mice at 12 months of age. Scale bars: 500 μm and 200 μm. **(B)** The right knee joints of Control and Glob-miR-23clus KO mice at 12 μmmonths of age (Control: $n = 11$, Glob-miR-23clus KO: $n = 13$) were assessed by OARSI scoring, meniscus scoring, synovitis scoring and ScB scoring system. The data was represented as median. Comparison of scoring data was performed by Mann-Whitney *U* test. **(C,D)** Knee joints from Control and Glob-miR-23clus KO mice were assessed by immunohistochemistry using anti-16^{INK4a} antibodies, and TUNEL staining ($n = 5$ per group). Scale bars: 200 μm. **(E,F)** Immunohistochemistry (ADAMTS5, MMP13, and type X Collagen) in articular cartilage of knee joints in Control and Glob-miR-23clus KO mice ($n = 5$ per group). Scale bars: 200 μm. All data was represented as mean ± SEM. Comparison of mean values was performed by Welch's *t*-test; $*p < .05$. n. s: non-significant difference.

maintaining articular cartilage state and anti-inflammation by *in vitro* studies (Akhtar et al., 2010; Hu et al., 2017; Zhou et al., 2017; Xu et al., 2018; Lv et al., 2020; Zhou et al., 2021). On the other hand, several reports suggest that miR-23a and miR-23b contribute to OA progression (Kang et al., 2016; Guo et al., 2018; Zhao et al., 2019). Thus, the role of each miRNA in miR-23a/b clusters is still controversial in OA pathogenesis. One of the reasons is that the deletion of a single miRNA in miRNA cluster may be compensated for by functionally redundant another miRNA in cluster. The present study demonstrated that miR-

23 a/b clusters-deletion have no critical role in the severity of OA with aging and following surgical trauma. This suggests that miR-23a/b clusters, composed of miR-23a, miR-23b, miR-24, miR-27a and miR-27b is not essential for cartilage homeostasis.

MiR-23a/b clusters were highly expressed in cartilage. Among them, miR-23a, miR-24, and miR-27a were significantly downregulated in OA chondrocytes. However, miR-23clus KO mice did not accelerate the severity of OA. In the screening of target genes for miR-23a/b clusters using multiomics analysis, 94 candidate genes were listed. The upregulated genes and proteins in miR-23clus KO chondrocytes might not only be candidate target genes for miR-23a/b clusters but also altered secondarily to compensate for the functionally complement genes due to the deficiency of miR-23a/b clusters in chondrocytes. However, the upregulated genes and proteins mean that they were not essentially associated with OA pathogenesis as shown by the phenotype of miR-23clus KO mice. Although we listed cartilage-miRNAs (Supplementary Table S4), functioning coordinately with other miRNAs might be a potential explanation for the lack of OA-like phenotype of miR-23a/b clusters deficiency in cartilage. Indeed, the expression level of OA-related genes might be coordinately regulated by multiple miRNAs that are highly expressed in cartilage. We can find a target gene for multiple miRNAs like this in OA-related genes from the database, TargetScan 8.0 (https://www.targetscan.org/vert_80/). For example, we found that cartilage-degrading enzyme, *Adamts5*, is a common target gene for miR-23a, miR-27a and miR-140 (Supplementary Table S6). Thus, the phenotype of double KO mice of miR-23a/b clusters and other cartilage-miRNA might be a potential explanation for fine-tuning the expression level of common target genes and causing OA-like pathological conditions. Currently, we are working on to further clarify the reason for the lack of the phenotype in the present study. In addition, previous reported target genes of miR-23, miR-24 and miR-27a such as *Runx2*, murine double minute 4 (*Mdm4*), *Smad3*, *Leptin* and *Mmp13* (Zhang et al., 2011; Zhang et al., 2012; Kang et al., 2016; Zhou et al., 2017; Li et al., 2018; Zhao et al., 2019; Xu et al., 2021) were not included among 94 candidate genes. The identification of target gene for miRNAs depends on the kinds of cell type, and endogenous target gene expression level under various conditions such as aging and inflammation in *in vitro* and *in vivo*. Furthermore, many target genes for miR-23a/b clusters have been identified by *in vitro* model using excessive miR-23a/b mimic or inhibitor. These factors might be one of the reasons.

Aging and age-related diseases have been characterized by the accumulation of senescent cells in various tissues including cartilage and are associated with age-related pathogenesis (Baker et al., 2016; Farr et al., 2017; Jeon et al., 2017). Glob-miR-23clus KO mice exhibited low bone density at 12 months of age. Although miR-24 is a negative regulator of the senescence marker $p16^{INK4a}$ (Philipot et al., 2014), Glob-miR-23clus KO mice did not show increased severity of OA. This lack of an OA phenotype is despite the fact that we observed some molecular and cellular changes (increased MMP13 and $p16^{INK4a}$-positive senescent cells in cartilage) in the Glob-miR-23clus KO mice with aging. A recent study reported that $p16^{INK4a}$ expression is a biomarker of dysfunctional chondrocytes but does not cause OA (Diekman et al., 2018). Our results may support that, and/or OA may develop at a later stage compared with aging-like phenotype such as osteopenia. Furthermore, the present study indicated that the deficiency of miR-23 a/b clusters in other tissues (other cells) except cartilage (chondrocytes), and in body fluids may have caused the impaired growth including skeletal growth with aging. Previously, tissue-specific miR-23a/b clusters deficient mice, such as vascular endothelial cells- and muscle-specific miR-23a/b clusters deficient mice, exhibit normal growth and have no dramatic effects on tissue or cell functions (Oikawa et al., 2018; Lee et al., 2019). In bone, miR-23a/b clusters inhibit osteogenesis by targeting *Runx2*, *Satb2*, *Sp7* (*Osterix*), and *Bmpr1b in vitro* (Hassan et al., 2010; Peng et al., 2017; Godfrey et al., 2018; Zhang et al., 2019). Global-miR-23a transgenic (Tg) mice revealed a limited role in bone formation and maintenance (Park et al., 2015). Osteoblast-specific miR-23a cluster Tg mice exhibit low bone mass through targeting of *Prdm16* (Zeng et al., 2017). On the other hand, male and female miR-23a cluster knockdown mice (homozygous miR-23a Cl^{ZIP} mice) died postnatally, and female miR-23a cluster knockdown mice (hetero zygous miR-23a Cl^{ZIP} mice) had increase bone density (Godfrey et al., 2018). The phenotype due to the difference of sex in miR-23clus KO mice should further be examined since only male mice were investigated in the present study. Furthermore, recently, exosomal miRNAs have attracted increasing attention because of their relation to the pathogenesis of various diseases as new mediators of tissue-to-tissue/cell-to-cell communication (Valadi et al., 2007; Mori et al., 2019). miR-23a from osteoclast-derived EVs suppress osteogenesis by targeting *Runx2* (Yang et al., 2020). From previous studies and the present study, however, aging-like phenotype with osteopenia in Glob-miR-23clus KO mice might be due to the impairment of endocrine and nervous system rather than derived from skeletal system-related cells such as chondrocytes, muscle cells, osteoblasts, osteocytes and osteoclasts. Furthermore, miR-23a/b clusters KO mice show decreased bone marrow cellularity and hematopoietic stem cell populations (Kurkewich et al., 2018). Thus, we should further examine what functions of miR-23a/b clusters including exosomal miRNAs is derived from which cells, and their target genes in order to reveal the mechanism of accelerated aging-like phenotype such as osteopenia in Glob-miR-23clus KO mice. These future results will open a new insight in aging mechanisms through the miR-23 a/b clusters.

Together, miR-23a and -23b clusters were highly expressed in various tissues including cartilage. However, loss-of-function studies using cartilage-specific- and global-miR-23clus KO mice demonstrated that the biomedical function of miR-23 a/b clusters in chondrocytes is not essential for OA pathogenesis.

Data availability statement

The datasets presented in this study can be found in online repositories. The names of the repository/repositories and accession number(s) can be found in the article/Supplementary Material.

Ethics statement

The studies involving human participants were reviewed and approved by Human tissue collection was approved by Human Subjects Committee of Scripps Research or Hiroshima University Hospital. The patients/participants provided their written informed consent to participate in this study. The animal study was reviewed and approved by All animal experiments were performed according to protocols approved by the institutional Animal Care and Use Committees at Hiroshima University.

Author contributions

YF, CD, and SM contributed to the conception and design of the study. YF, CD, YS, DY, TN, MI, NK, KI, and TA performed the experiments. YF, CD, YS, and SM contribute to the analysis and interpretation of data. YF, CD, NA, ML, and SM contributed to draft manuscript. All authors approved the submitted manuscript.

Funding

This research was supported by MEXT/JPS KAKENHI for Scientific Research (B) Grant 15H04959 (SM), 17H04314 (NA), 19H03785 (SM), Takeda Science Foundation (SM), Mochida memorial foundation (SM), and Suzuken memorial foundation (SM). The study sponsors had no role in the study design, collection, analysis and interpretation of data; the writing of the manuscript; or the decision to submit the manuscript for publication.

Acknowledgments

We thank T. Miyata, E. Ueda, M, DVM. A. Saito, Y. Takagi and K. Koike for excellent technical support. A part of this work was carried out at the Analysis Center of Life Science and Research Facilities for Laboratory Animal Science, Natural Science Center for Basic Research and Development (N-BARD), Hiroshima University.

Conflict of interest

The authors declare that the research was conducted in the absence of any commercial or financial relationships that could be construed as a potential conflict of interest.

Publisher's note

Supplementary material

The Supplementary Material for this article can be found online at: https://www.frontiersin.org/articles/10.3389/fcell.2022.1043259/full#supplementary-material

References

Akhtar, N., Rasheed, Z., Ramamurthy, S., Anbazhagan, A. N., Voss, F. R., and Haqqi, T. M. (2010). MicroRNA-27b regulates the expression of matrix metalloproteinase 13 in human osteoarthritis chondrocytes. *Arthritis Rheum.* 62 (5), 1361–1371. doi:10.1002/art.27329

Baker, D. J., Childs, B. G., Durik, M., Wijers, M. E., Sieben, C. J., Zhong, J., et al. (2016). Naturally occurring p16(Ink4a)-positive cells shorten healthy lifespan. *Nature* 530 (7589), 184–189. doi:10.1038/nature16932

Bartel, D. P. (2018). Metazoan MicroRNAs. *Cell* 173 (1), 20–51. doi:10.1016/j.cell.2018.03.006

Castanheira, C., Anderson, J. R., Fang, Y., Milner, P. I., Goljanek-Whysall, K., House, L., et al. (2021). Mouse microRNA signatures in joint ageing and post-traumatic osteoarthritis. *Osteoarthr. Cartil. Open* 3 (4), 100186. doi:10.1016/j.ocarto.2021.100186

Castro-Villegas, C., Perez-Sanchez, C., Escudero, A., Filipescu, I., Verdu, M., Ruiz-Limon, P., et al. (2015). Circulating miRNAs as potential biomarkers of therapy effectiveness in rheumatoid arthritis patients treated with anti-TNFα. *Arthritis Res. Ther.* 17, 49. doi:10.1186/s13075-015-0555-z

Chang, S. H., Mori, D., Kobayashi, H., Mori, Y., Nakamoto, H., Okada, K., et al. (2019). Excessive mechanical loading promotes osteoarthritis through the gremlin-1-NF-κB pathway. *Nat. Commun.* 10 (1), 1442. doi:10.1038/s41467-019-09491-5

Cicuttini, F. M., and Wluka, A. E. (2014). Osteoarthritis: Is OA a mechanical or systemic disease? *Nat. Rev. Rheumatol.* 10 (9), 515–516. doi:10.1038/nrrheum.2014.114

Diekman, B. O., Sessions, G. A., Collins, J. A., Knecht, A. K., Strum, S. L., Mitin, N. K., et al. (2018). Expression of p16(INK) (4a) is a biomarker of chondrocyte aging but does not cause osteoarthritis. *Aging Cell* 17 (4), e12771. doi:10.1111/acel.12771

Duan, L., Liang, Y., Xu, X., Xiao, Y., and Wang, D. (2020). Recent progress on the role of miR-140 in cartilage matrix remodelling and its implications for osteoarthritis treatment. *Arthritis Res. Ther.* 22 (1), 194. doi:10.1186/s13075-020-02290-0

Endisha, H., Rockel, J., Jurisica, I., and Kapoor, M. (2018). The complex landscape of microRNAs in articular cartilage: Biology, pathology, and therapeutic targets. *JCI Insight* 3 (17), e121630. doi:10.1172/jci.insight.121630

Farr, J. N., Xu, M., Weivoda, M. M., Monroe, D. G., Fraser, D. G., Onken, J. L., et al. (2017). Targeting cellular senescence prevents age-related bone loss in mice. *Nat. Med.* 23 (9), 1072–1079. doi:10.1038/nm.4385

Furuta, T., Miyaki, S., Ishitobi, H., Ogura, T., Kato, Y., Kamei, N., et al. (2016). Mesenchymal stem cell-derived exosomes promote fracture healing in a mouse model. *Stem Cells Transl. Med.* 5 (12), 1620–1630. doi:10.5966/sctm.2015-0285

Garavelli, S., Bruzzaniti, S., Tagliabue, E., Di Silvestre, D., Prattichizzo, F., Mozzillo, E., et al. (2020). Plasma circulating miR-23~27~24 clusters correlate with the immunometabolic derangement and predict C-peptide loss in children with type 1 diabetes. *Diabetologia* 63 (12), 2699–2712. doi:10.1007/s00125-020-05237-x

Glasson, S. S., Chambers, M. G., Van Den Berg, W. B., and Little, C. B. (2010). The OARSI histopathology initiative - recommendations for histological assessments of osteoarthritis in the mouse. *Osteoarthr. Cartil.* 18, S17–S23. doi:10.1016/j.joca.2010.05.025

Godfrey, T. C., Wildman, B. J., Beloti, M. M., Kemper, A. G., Ferraz, E. P., Roy, B., et al. (2018). The microRNA-23a cluster regulates the developmental HoxA cluster function during osteoblast differentiation. *J. Biol. Chem.* 293 (45), 17646–17660. doi:10.1074/jbc.RA118.003052

Guo, Y., Min, Z., Jiang, C., Wang, W., Yan, J., Xu, P., et al. (2018). Downregulation of HS6ST2 by miR-23b-3p enhances matrix degradation through p38 MAPK pathway in osteoarthritis. *Cell Death Dis.* 9 (6), 699. doi:10.1038/s41419-018-0729-0

Hassan, M. Q., Gordon, J. A., Beloti, M. M., Croce, C. M., van Wijnen, A. J., Stein, J. L., et al. (2010). A network connecting Runx2, SATB2, and the miR-23a~27a~24-2 cluster regulates the osteoblast differentiation program. *Proc. Natl. Acad. Sci. U. S. A.* 107 (46), 19879–19884. doi:10.1073/pnas.1007698107

Hu, J., Zhai, C., Hu, J., Li, Z., Fei, H., Wang, Z., et al. (2017). MiR-23a inhibited IL-17-mediated proinflammatory mediators expression via targeting IKKα in articular chondrocytes. *Int. Immunopharmacol.* 43, 1–6. doi:10.1016/j.intimp.2016.11.031

Huang, J., Zhao, L., Fan, Y., Liao, L., Ma, P. X., Xiao, G., et al. (2019). The microRNAs miR-204 and miR-211 maintain joint homeostasis and protect against osteoarthritis progression. *Nat. Commun.* 10 (1), 2876. doi:10.1038/s41467-019-10753-5

Ishitobi, H., Sanada, Y., Kato, Y., Ikuta, Y., Shibata, S., Yamasaki, S., et al. (2018). Carnosic acid attenuates cartilage degeneration through induction of heme oxygenase-1 in human articular chondrocytes. *Eur. J. Pharmacol.* 830, 1–8. doi:10.1016/j.ejphar.2018.04.018

Ito, Y., Matsuzaki, T., Ayabe, F., Mokuda, S., Kurimoto, R., Matsushima, T., et al. (2021). Both microRNA-455-5p and -3p repress hypoxia-inducible factor-2α expression and coordinately regulate cartilage homeostasis. *Nat. Commun.* 12 (1), 4148. doi:10.1038/s41467-021-24460-7

Jeon, O. H., Kim, C., Laberge, R. M., Demaria, M., Rathod, S., Vasserot, A. P., et al. (2017). Local clearance of senescent cells attenuates the development of post-traumatic osteoarthritis and creates a pro-regenerative environment. *Nat. Med.* 23 (6), 775–781. doi:10.1038/nm.4324

June, R. K., Liu-Bryan, R., Long, F., and Griffin, T. M. (2016). Emerging role of metabolic signaling in synovial joint remodeling and osteoarthritis. *J. Orthop. Res.* 34 (12), 2048–2058. doi:10.1002/jor.23420,

Kamekura, S., Hoshi, K., Shimoaka, T., Chung, U., Chikuda, H., Yamada, T., et al. (2005). Osteoarthritis development in novel experimental mouse models induced by knee joint instability. *Osteoarthr. Cartil.* 13 (7), 632–641. doi:10.1016/j.joca.2005.03.004

Kang, L., Yang, C., Song, Y., Liu, W., Wang, K., Li, S., et al. (2016). MicroRNA-23a-3p promotes the development of osteoarthritis by directly targeting SMAD3 in chondrocytes. *Biochem. Biophys. Res. Commun.* 478 (1), 467–473. doi:10.1016/j.bbrc.2016.06.071

Kawashima, Y., Watanabe, E., Umeyama, T., Nakajima, D., Hattori, M., Honda, K., et al. (2019). Optimization of data-independent acquisition mass spectrometry for deep and highly sensitive proteomic analysis. *Int. J. Mol. Sci.* 20 (23), 5932. doi:10.3390/ijms20235932

Krenn, V., Morawietz, L., Haupl, T., Neidel, J., Petersen, I., and Konig, A. (2002). Grading of chronic synovitis--a histopathological grading system for molecular and diagnostic pathology. *Pathol. Res. Pract.* 198 (5), 317–325. doi:10.1078/0344-0338-5710261

Kurkewich, J. L., Boucher, A., Klopfenstein, N., Baskar, R., Kapur, R., and Dahl, R. (2018). The mirn23a and mirn23b microrna clusters are necessary for proper hematopoietic progenitor cell production and differentiation. *Exp. Hematol.* 59, 14–29. doi:10.1016/j.exphem.2017.12.007

Kwok, J., Onuma, H., Olmer, M., Lotz, M. K., Grogan, S. P., and D'Lima, D. D. (2016). Histopathological analyses of murine menisci: Implications for joint aging and osteoarthritis. *Osteoarthr. Cartil.* 24 (4), 709–718. doi:10.1016/j.joca.2015.11.006

Lee, M., Wada, S., Oikawa, S., Suzuki, K., Ushida, T., and Akimoto, T. (2019). Loss of microRNA-23-27-24 clusters in skeletal muscle is not influential in skeletal muscle development and exercise-induced muscle adaptation. *Sci. Rep.* 9 (1), 1092. doi:10.1038/s41598-018-37765-3

Li, X., He, P., Li, Z., Wang, H., Liu, M., Xiao, Y., et al. (2018). Interleukin-1β-mediated suppression of microRNA-27a-3p activity in human cartilage via mapk and NF-κB pathways: A potential mechanism of osteoarthritis pathogenesis. *Mol. Med. Rep.* 18 (1), 541–549. doi:10.3892/mmr.2018.8970

Liu, Y., Tan, J., Ou, S., Chen, J., and Chen, L. (2019). Adipose-derived exosomes deliver miR-23a/b to regulate tumor growth in hepatocellular cancer by targeting the VHL/HIF axis. *J. Physiol. Biochem.* 75 (3), 391–401. doi:10.1007/s13105-019-00692-6

Loeser, R. F., Goldring, S. R., Scanzello, C. R., and Goldring, M. B. (2012). Osteoarthritis: A disease of the joint as an organ. *Arthritis Rheum.* 64 (6), 1697–1707. doi:10.1002/art.34453

Lv, S., Xu, J., Chen, L., Wu, H., Feng, W., Zheng, Y., et al. (2020). MicroRNA-27b targets CBFB to inhibit differentiation of human bone marrow mesenchymal stem cells into hypertrophic chondrocytes. *Stem Cell Res. Ther.* 11 (1), 392. doi:10.1186/s13287-020-01909-y

Maier, R., Ganu, V., and Lotz, M. (1993). Interleukin-11, an inducible cytokine in human articular chondrocytes and synoviocytes, stimulates the production of the tissue inhibitor of metalloproteinases. *J. Biol. Chem.* 268 (29), 21527–21532. doi:10.1016/s0021-9258(20)80573-0

Matsumura, H., Hasuwa, H., Inoue, N., Ikawa, M., and Okabe, M. (2004). Lineage-specific cell disruption in living mice by Cre-mediated expression of diphtheria toxin A chain. *Biochem. Biophys. Res. Commun.* 321 (2), 275–279. doi:10.1016/j.bbrc.2004.06.139

Mihanfar, A., Shakouri, S. K., Khadem-Ansari, M. H., Fattahi, A., Latifi, Z., Nejabati, H. R., et al. (2020). Exosomal miRNAs in osteoarthritis. *Mol. Biol. Rep.* 47 (6), 4737–4748. doi:10.1007/s11033-020-05443-1

Miyaki, S., and Lotz, M. K. (2018). Extracellular vesicles in cartilage homeostasis and osteoarthritis. *Curr. Opin. Rheumatol.* 30 (1), 129–135. doi:10.1097/BOR.0000000000000454

Miyaki, S., Nakasa, T., Otsuki, S., Grogan, S. P., Higashiyama, R., Inoue, A., et al. (2009). MicroRNA-140 is expressed in differentiated human articular chondrocytes and modulates interleukin-1 responses. *Arthritis Rheum.* 60 (9), 2723–2730. doi:10.1002/art.24745

Miyaki, S., Sato, T., Inoue, A., Otsuki, S., Ito, Y., Yokoyama, S., et al. (2010). MicroRNA-140 plays dual roles in both cartilage development and homeostasis. *Genes Dev.* 24 (11), 1173–1185. doi:10.1101/gad.1915510

Mori, M. A., Ludwig, R. G., Garcia-Martin, R., Brandao, B. B., and Kahn, C. R. (2019). Extracellular miRNAs: From biomarkers to mediators of physiology and disease. *Cell Metab.* 30 (4), 656–673. doi:10.1016/j.cmet.2019.07.011

Nagira, K., Ikuta, Y., Shinohara, M., Sanada, Y., Omoto, T., Kanaya, H., et al. (2020). Histological scoring system for subchondral bone changes in murine models of joint aging and osteoarthritis. *Sci. Rep.* 10 (1), 10077. doi:10.1038/s41598-020-66979-7

Nakamura, Y., Inloes, J. B., Katagiri, T., and Kobayashi, T. (2011). Chondrocyte-specific microRNA-140 regulates endochondral bone development and targets Dnpep to modulate bone morphogenetic protein signaling. *Mol. Cell Biol.* 31 (14), 3019–3028. doi:10.1128/MCB.05178-11

Oikawa, S., Wada, S., Lee, M., Maeda, S., and Akimoto, T. (2018). Role of endothelial microRNA-23 clusters in angiogenesis *in vivo*. *Am. J. Physiol. Heart Circ. Physiol.* 315 (4), H838–H846. doi:10.1152/ajpheart.00742.2017

Ovchinnikov, D. A., Deng, J. M., Ogunrinu, G., and Behringer, R. R. (2000). Col2a1-directed expression of Cre recombinase in differentiating chondrocytes in transgenic mice. *Genesis* 26 (2), 145–146. doi:10.1002/(sici)1526-968x(200002)26:2<145::aid-gene14>3.0.co;2-c

Park, J., Wada, S., Ushida, T., and Akimoto, T. (2015). The microRNA-23a has limited roles in bone formation and homeostasis *in vivo*. *Physiol. Res.* 64 (5), 711–719. doi:10.33549/physiolres.932901

Peng, W., Zhu, S., Li, X., Weng, J., and Chen, S. (2017). miR-27b-3p suppressed osteogenic differentiation of maxillary sinus membrane stem cells by targeting Sp7. *Implant Dent.* 26 (4), 492–499. doi:10.1097/ID.0000000000000637

Philipot, D., Guerit, D., Platano, D., Chuchana, P., Olivotto, E., Espinoza, F., et al. (2014). p16INK4a and its regulator miR-24 link senescence and chondrocyte terminal differentiation-associated matrix remodeling in osteoarthritis. *Arthritis Res. Ther.* 16 (1), R58. doi:10.1186/ar4494

Valadi, H., Ekstrom, K., Bossios, A., Sjostrand, M., Lee, J. J., and Lotvall, J. O. (2007). Exosome-mediated transfer of mRNAs and microRNAs is a novel mechanism of genetic exchange between cells. *Nat. Cell Biol.* 9 (6), 654–659. doi:10.1038/ncb1596

Wang, H., Zhang, H., Sun, Q., Wang, Y., Yang, J., Yang, J., et al. (2017). Intra-articular delivery of antago-miR-483-5p inhibits osteoarthritis by modulating matrilin 3 and tissue inhibitor of metalloproteinase 2. *Mol. Ther.* 25 (3), 715–727. doi:10.1016/j.ymthe.2016.12.020

Xu, J., Lv, S., Hou, Y., Xu, K., Sun, D., Zheng, Y., et al. (2018). miR-27b promotes type II collagen expression by targetting peroxisome proliferator-activated receptor-γ2 during rat articular chondrocyte differentiation. *Biosci. Rep.* 38 (1), BSR20171109. doi:10.1042/BSR20171109

Xu, J., Qian, X., and Ding, R. (2021). MiR-24-3p attenuates IL-1β-induced chondrocyte injury associated with osteoarthritis by targeting BCL2L12. *J. Orthop. Surg. Res.* 16 (1), 371. doi:10.1186/s13018-021-02378-6

Yang, J. X., Xie, P., Li, Y. S., Wen, T., and Yang, X. C. (2020). Osteoclast-derived miR-23a-5p-containing exosomes inhibit osteogenic differentiation by regulating Runx2. *Cell Signal* 70, 109504. doi:10.1016/j.cellsig.2019.109504

Zeng, H. C., Bae, Y., Dawson, B. C., Chen, Y., Bertin, T., Munivez, E., et al. (2017). MicroRNA miR-23a cluster promotes osteocyte differentiation by regulating TGF-beta signalling in osteoblasts. *Nat. Commun.* 8, 15000. doi:10.1038/ncomms15000

Zhang, Y., Li, S., Yuan, S., Zhang, H., and Liu, J. (2019). MicroRNA-23a inhibits osteogenesis of periodontal mesenchymal stem cells by targeting bone morphogenetic protein signaling. *Arch. Oral Biol.* 102, 93–100. doi:10.1016/j.archoralbio.2019.04.001

Zhang, Y., Xie, R. L., Croce, C. M., Stein, J. L., Lian, J. B., van Wijnen, A. J., et al. (2011). A program of microRNAs controls osteogenic lineage progression by targeting transcription factor Runx2. *Proc. Natl. Acad. Sci. U. S. A.* 108 (24), 9863–9868. doi:10.1073/pnas.1018493108

Zhang, Y., Xie, R. L., Gordon, J., LeBlanc, K., Stein, J. L., Lian, J. B., et al. (2012). Control of mesenchymal lineage progression by microRNAs targeting skeletal gene regulators Trps1 and Runx2. *J. Biol. Chem.* 287 (26), 21926–21935. doi:10.1074/jbc.M112.340398

Zhao, Z., Guan, J. Z., Wu, M., Lai, G. H., and Zhu, Z. L. (2019). Downregulation of microRNA-23b protects against ischemia-reperfusion injury via p53 signaling pathway by upregulating MDM4 in rats. *J. Cell Biochem.* 120 (3), 4599–4612. doi:10.1002/jcb.27748

Zhou, B., Li, H., and Shi, J. (2017). miR-27 inhibits the NF-κB signaling pathway by targeting leptin in osteoarthritic chondrocytes. *Int. J. Mol. Med.* 40 (2), 523–530. doi:10.3892/ijmm.2017.3021

Zhou, L., Gu, M., Ma, X., Wen, L., Zhang, B., Lin, Y., et al. (2021). Long non-coding RNA PCAT-1 regulates apoptosis of chondrocytes in osteoarthritis by sponging miR-27b-3p. *J. Bone Min. Metab.* 39 (2), 139–147. doi:10.1007/s00774-020-01128-8

Zhou, Y., Zhou, B., Pache, L., Chang, M., Khodabakhshi, A. H., Tanaseichuk, O., et al. (2019). Metascape provides a biologist-oriented resource for the analysis of systems-level datasets. *Nat. Commun.* 10 (1), 1523. doi:10.1038/s41467-019-09234-6

frontiers

Supplementary Material

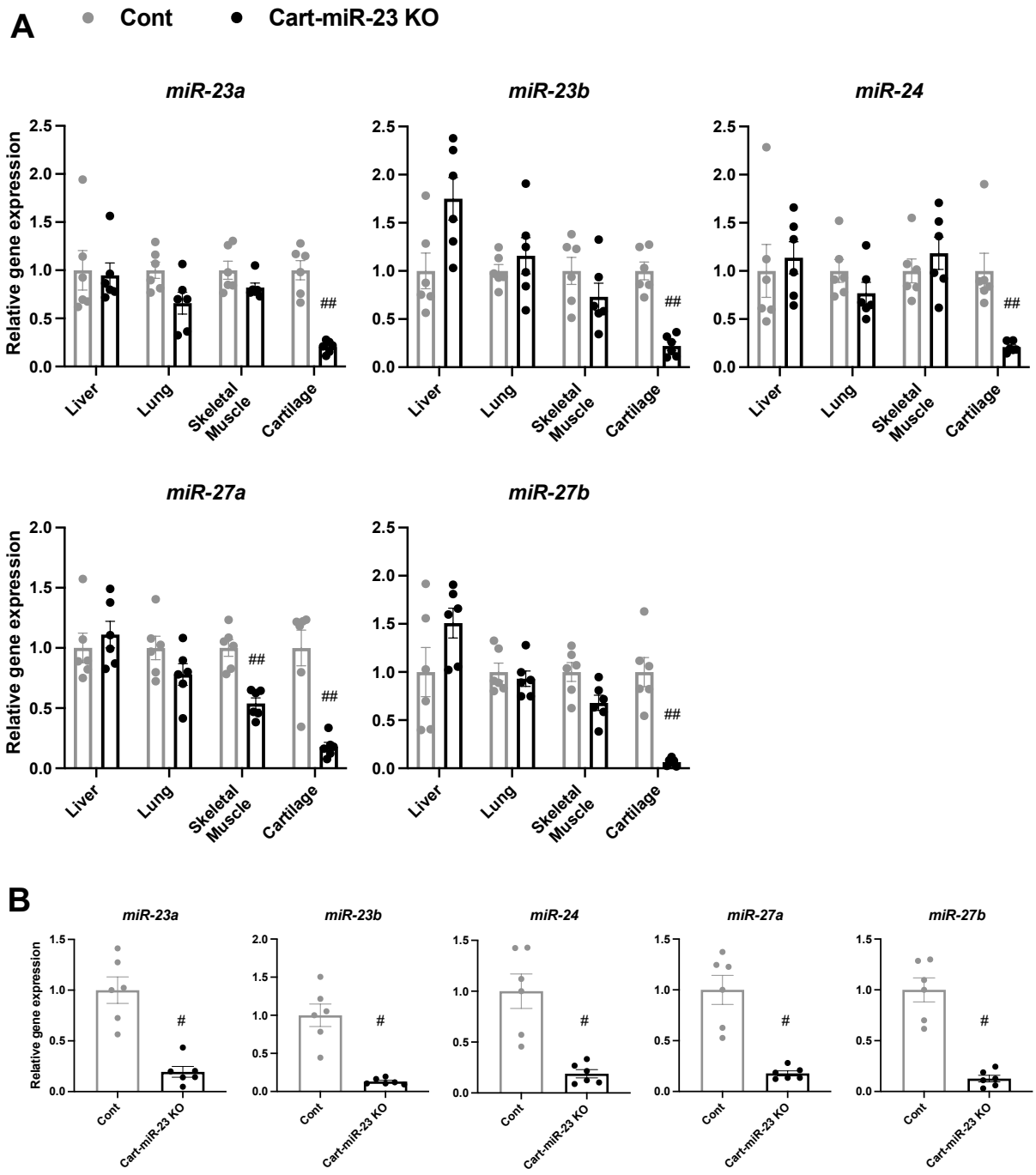

Fig. S1 Validation of cartilage-specific miR-23a/b clusters deficiency in Cart-miR-23clus KO mice.

A) Real-time analysis showed the expression of miR-23a/b clusters in liver, lung, skeletal muscle, and articular cartilage from Control and Cart-miR-23clus KO mice at 4 weeks of age. **B**) The expression of miR-23a/b clusters in articular chondrocytes from Control and Cart-miR-23clus KO mice. All data are represented as mean ± SEM. Comparisons of expression level were performed by Mann-Whitney tests in each tissue. Holm-Sidak corrections were applied to correct for multiple comparisons. $^{\#}P<0.05$, $^{\#\#}P<0.01$. n=6 per group.

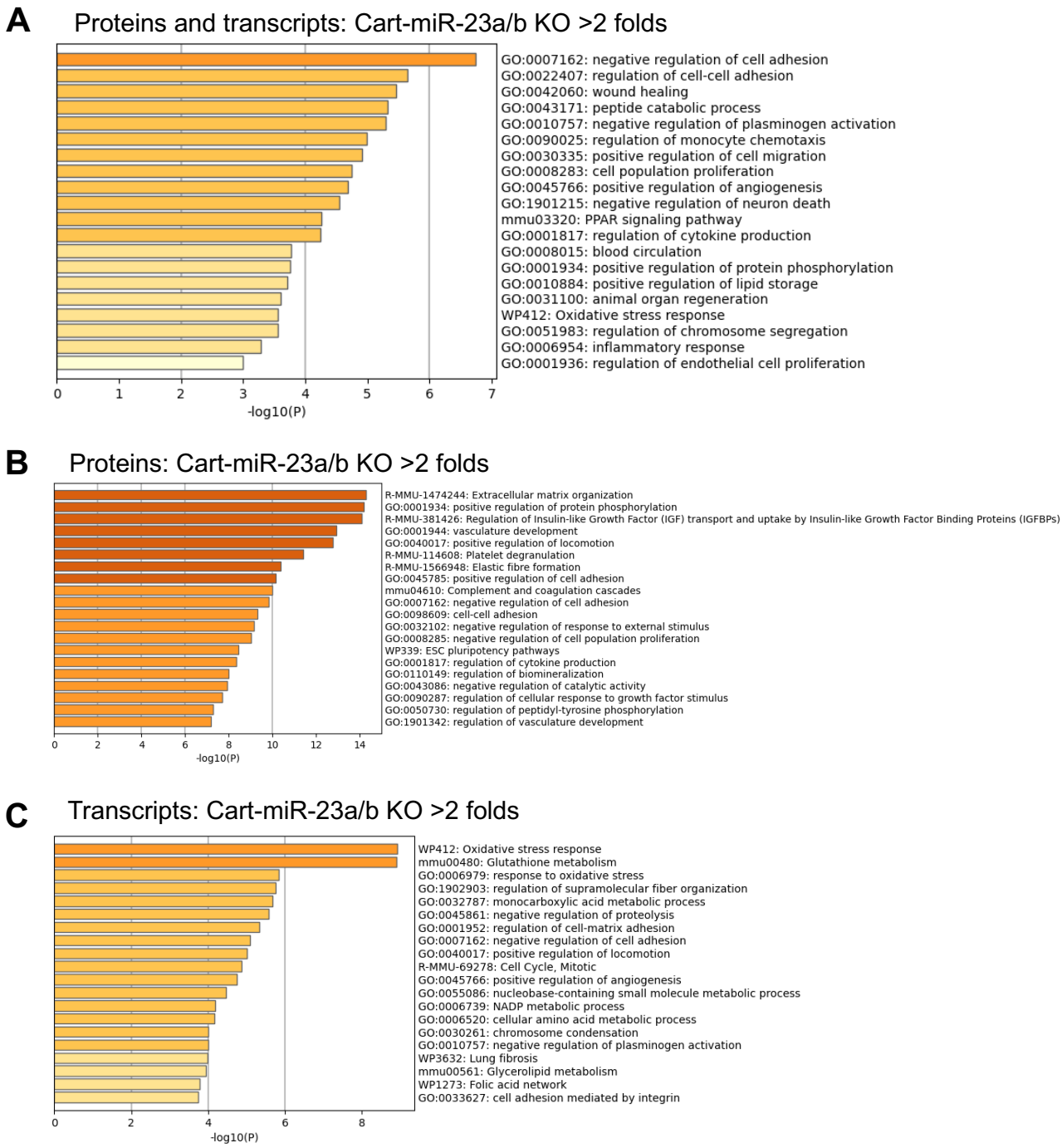

Fig. S2 Top 20 gene ontology enrichment analysis terms for the genes which **A)** proteins and transcripts are both have been upregulated (>2 folds) **B)** proteins have been upregulated (>2 folds) **C)** transcripts have been upregulated (>2 folds) in articular chondrocytes from Cart-miR-23a/b KO mouse compared to Control mouse.

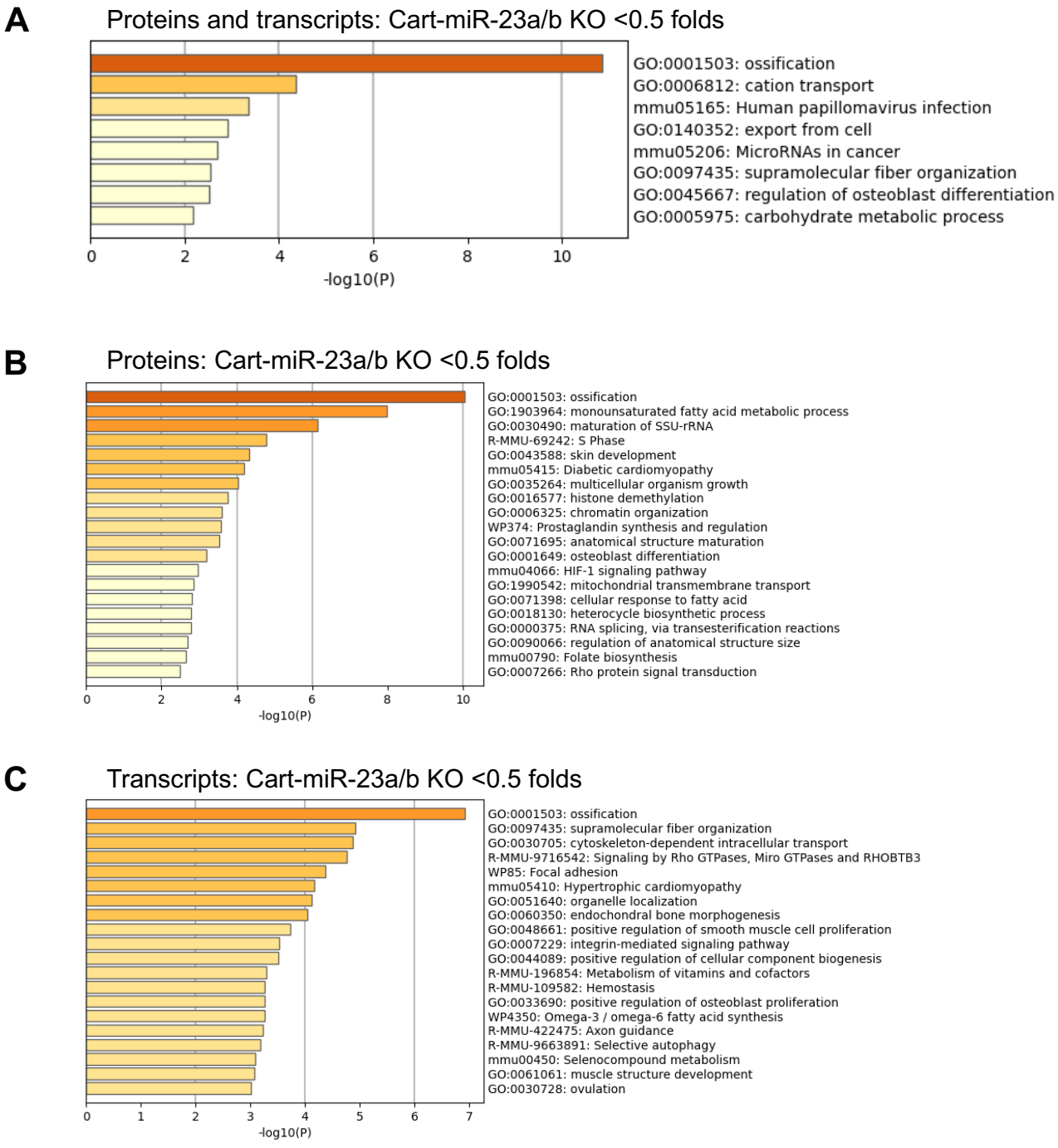

Fig. S3 Top gene ontology enrichment analysis terms for the genes which **A)** proteins and transcripts are both have been downregulated (<0.5 folds) **B)** proteins have been downregulated (<0.5 folds) **C)** transcripts have been downregulated (<0.5 folds) in articular chondrocytes from Cart-miR-23a/b KO mouse compared to Control mouse.

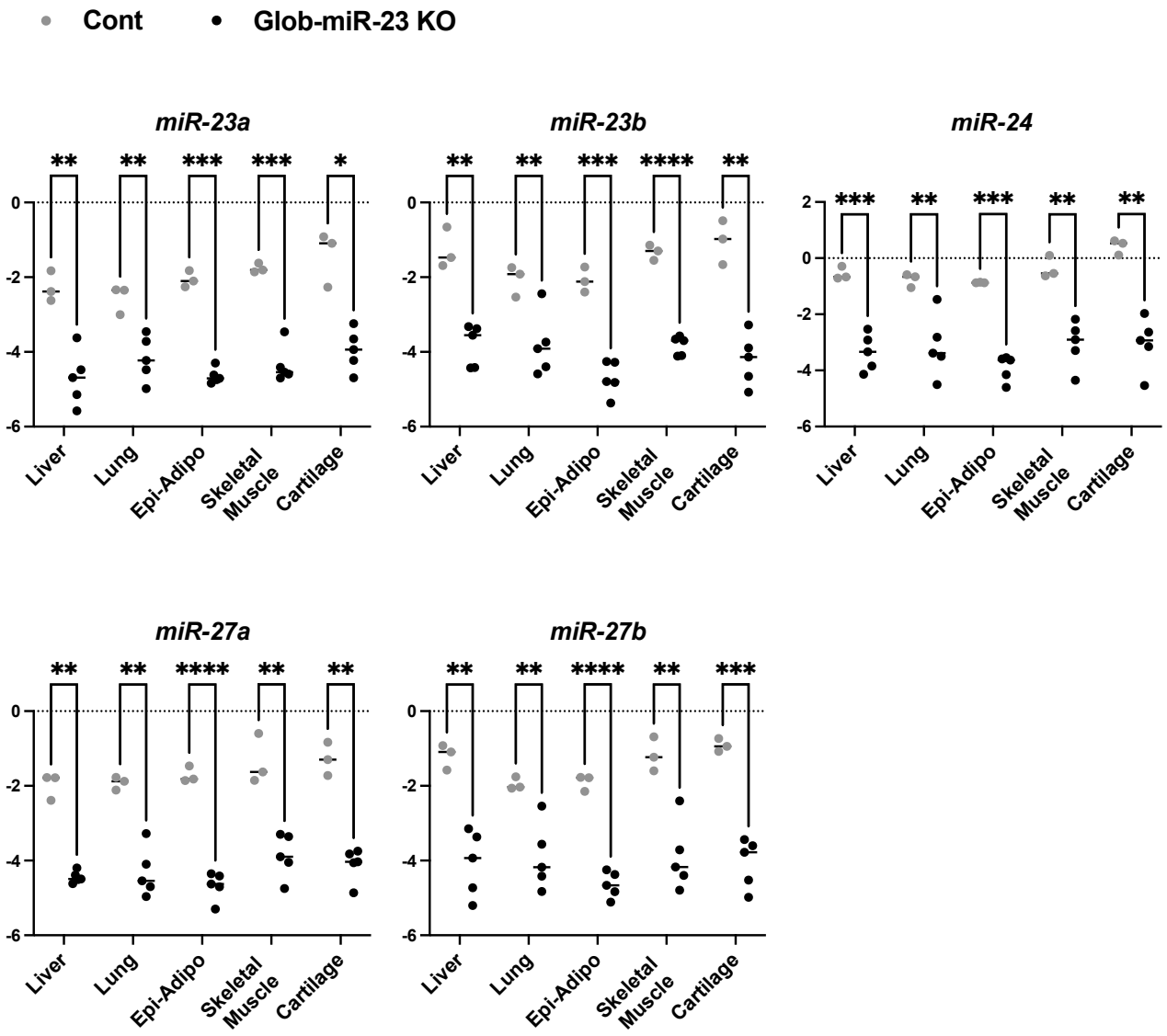

Fig. S4 Validation of miR-23a/b clusters deficiency in various tissues of Glob-miR-23clus KO mice.

Real-time PCR analysis showed the expression of miR-23a/b clusters in liver, lung, epididymal adipose tissue, skeletal muscle, and articular cartilage from Control (n=3) and Glob-miR-23clus KO mice (n=5) at 4 weeks of age. All data are represented as mean ± SEM. Comparisons of expression level were performed by multiple welch test. $^{*}P<0.05$, $^{**}P<0.01$, $^{***}P<0.001$, $^{****}P<0.0001$.

Table. S1

	Primer sequence
miR-23a cluster*	F: GCTCCAACCTTCCTACGGATCGATGC
	R-1: CCTGCCTCTACCTCTGGAGTCTAGGA
	R-2: GTGGTGCAGCTGGTATTCCCAAACTC
miR-23b cluster*	F: TGCCCCCTGAGTGAGCAAATCC
	R-1: TGGCTTGCCTGTGACCAAGCAT
	R-2: GGTGTCCTTCATTGAATGACTGCC
Cre recombinase	F: GCATTACCGGTCGATGCAACGAGTGATGAG
	R: GAGTGAACGAACCTGGTCGAAATCAGTGCG

*For the genotyping of the miR-23a or miR-23b cluster, primer-F and primer-R-1 were used for the Cart:miR-23clusKO mice and the combinations of primer-F with primer-R-1 and primer-F with primer-R-2 were used for the Glob-miR-23clusKO mice.

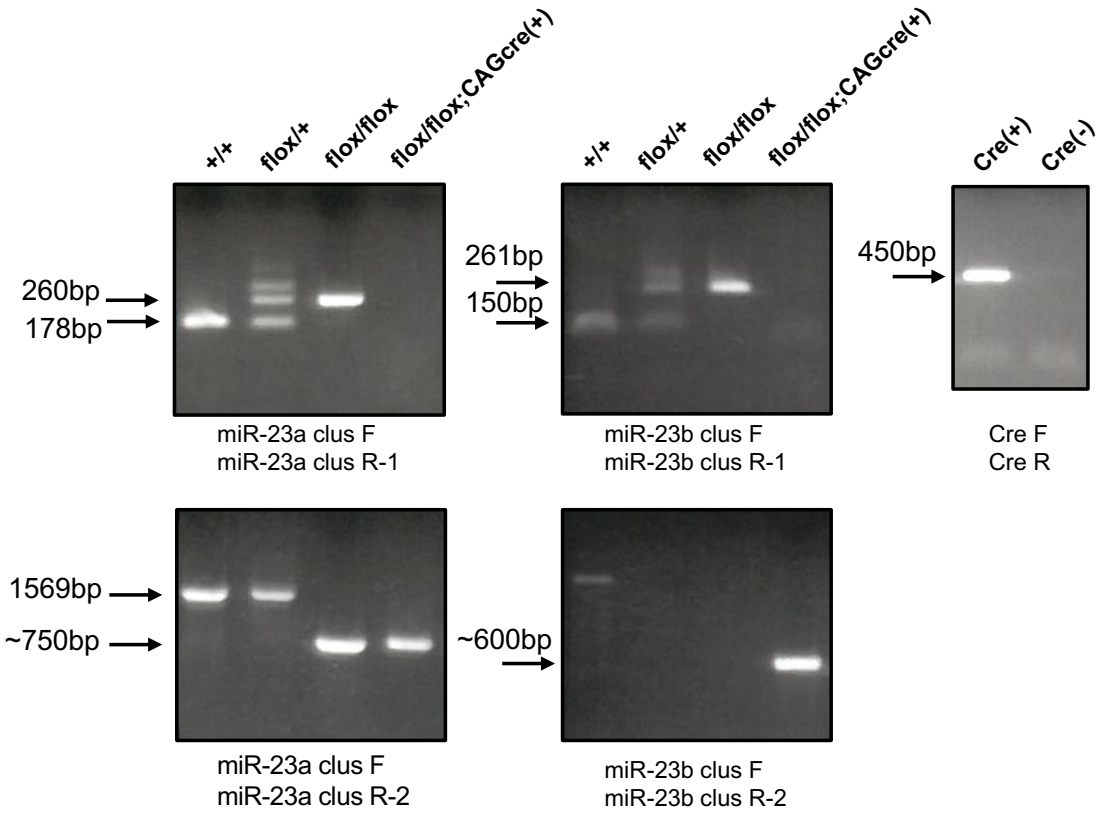

Table. S2

Gene Name	Assay ID
Col2a1	Mm01309565m1
Acan	Mm00545807m1
Mmp13	Mm00439491m1
Adamts5	Mm00478620m1
Il6	Mm00446190m1
Runx2	Mm00446190m1
Gapdh	Mm99999915g1
miR-23a-3p	RT/TM000399
miR-23b-3p	RT/TM000400
miR-24-3p	RT/TM000402
miR-27a-3p	RT/TM000408
miR-27b-3p	RT/TM000409
miR-140-5p	RT/TM000462
miR-455-3p	RT/TM002244
miR-455-5p	RT/TM001280
U6 snRNA	RT/TM001973

Real time PCR was performed with the TaqMan Gene Expression Assay probes

Table. S3

Antibody	Catalog Number	Manufacturer
COX2 (mouse, monoclonal)	sc-376861	Santa Cruz Biotechnology
iNOS (rabbit, polyclonal)	ab15323	Abcam
MMP13 (mouse, monoclonal)	MA5-14238	Thermo Fisher Scientific
SMAD3 (rabbit, monoclonal)	ab40854	Abcam
GAPDH (mouse, monoclonal)	015-25473	FUJIFILM Wako

Table. S4

	Chondrocyte		Cho-EVs	
microRNA	**Rank**	**Normalized Counts**	**Rank**	**Normalized Counts**
hsa-let-7a-5p	1	47048.64	5	12162.12
hsa-miR-125b-5p	2	35194.21	2	35106.55
hsa-miR-4454	3	26155.59	1	49397.53
hsa-let-7b-5p	4	21205.61	12	4336.57
hsa-miR-21-5p	5	20252.24	3	17950.79
hsa-miR-23a-3p	**6**	**13823.68**	**4**	**15808.79**
hsa-miR-29b-3p	7	13301.61	14	3962.05
hsa-let-7g-5p	8	7865.05	15	3193.30
hsa-miR-100-5p	9	7533.65	8	5939.79
hsa-miR-99a-5p	10	5992.56	12	4336.57
hsa-miR-720	11	5370.90	6	7096.21
hsa-miR-221-3p	12	5224.52	24	2293.13
hsa-miR-199a-3p+hsa-miR-199b-3p	13	4641.19	9	5210.46
hsa-miR-222-3p	14	4160.89	11	4737.38
hsa-miR-27b-3p	**15**	**4019.85**	**18**	**2904.19**
hsa-miR-15b-5p	16	3885.41	20	2509.96
hsa-miR-23b-3p	**17**	**3869.70**	**16**	**3134.16**
hsa-miR-15a-5p	18	3536.10	22	2345.69
hsa-miR-22-3p	19	3050.78	21	2385.12
hsa-miR-125a-5p	20	2810.47	32	1373.25
hsa-miR-191-5p	21	2556.97	19	2825.34
hsa-miR-374a-5p	22	2547.24	26	1951.46
hsa-miR-26a-5p	23	2530.90	42	762.19
hsa-miR-148a-3p	24	2329.55	23	2339.12
hsa-miR-199a-5p	25	2218.98	27	1866.04
hsa-miR-376a-3p	26	1856.48	17	3055.31
hsa-miR-29a-3p	27	1789.57	29	1662.35
hsa-miR-16-5p	28	1717.63	28	1714.92
hsa-miR-337-5p	29	1683.71	31	1438.95
hsa-miR-140-5p	**30**	**1445.29**	**36**	**1136.71**
hsa-let-7i-5p	31	1313.67	46	670.20
hsa-let-7c	32	1133.99	58	473.08
hsa-miR-34a-5p	33	1117.03	51	525.65
hsa-miR-376c	34	1084.04	33	1327.25
hsa-miR-361-5p	35	1059.54	40	834.46
hsa-miR-199b-5p	36	1042.58	52	519.07
hsa-let-7e-5p	37	1042.27	70	341.67
hsa-miR-377-3p	38	882.69	30	1550.65
hsa-let-7f-5p	39	838.71	94	243.11
hsa-miR-130a-3p	40	809.50	37	1005.30
hsa-miR-382-5p	41	718.40	56	479.65
hsa-miR-155-5p	42	712.12	778	6.57
hsa-miR-106a-5p+hsa-miR-17-5p	43	681.96	71	335.10
hsa-miR-127-3p	44	626.99	43	729.33
hsa-miR-24-3p	**45**	**626.36**	**47**	**663.63**
…	…	…	…	…
hsa-miR-27a-3p	**98**	**167.74**	**126**	**164.26**

Cho-EVs: Chondrocyte-derived extracellular vehicles

Table. S5

	Mass Spectrometry (Identified Peptide Count)			RNA-seq (TPM)		
Gene name	**Cont**	**Cart-miR-23 KO**	**Fold Change**	**Cont**	**Cart-miR-23 KO**	**Fold Change**
Hmox1	447277000	1479628000	3.31	53.07	153.81	2.90
Serpine2	394245800	792757500	2.01	370.31	954.20	2.58
Serpinb1a	235063600	512885100	2.18	17.47	45.60	2.61
Gpnmb	184437900	429767000	2.33	125.39	343.42	2.74
Maoa	170023800	492563200	2.90	4.59	29.34	6.39
Plin4	148102900	420612600	2.84	12.81	45.97	3.59
Tpm2	136333500	339893200	2.49	61.33	124.83	2.04
Tagln	125071800	769259900	6.15	1.80	24.45	13.58
Ass1	73640130	196621700	2.67	2.82	12.43	4.40
Erap1	70216530	141026100	2.01	2.88	7.47	2.59
Aldh1a1	68154590	239258900	3.51	99.69	277.79	2.79
Fabp4	66201750	245077400	3.70	60.89	262.29	4.31
Mttp	48886180	106763900	2.18	2.42	5.58	2.31
Anpep	46278680	154543800	3.34	3.03	8.88	2.94
Lox	45187450	346526700	7.67	244.49	981.62	4.01
Emb	41188020	82608200	2.01	402.69	977.26	2.43
Icam1	26620030	474050000	17.81	11.73	79.41	6.77
Pdlim4	25021980	76676650	3.06	12.15	41.01	3.38
C3	22629220	49426810	2.18	0.56	3.28	5.87
Enpep	22315770	59819150	2.68	0.46	2.27	4.95
Gfer	21487370	44308620	2.06	57.62	142.16	2.47
Serpine1	20536510	67098690	3.27	40.05	85.40	2.13
Synm	20516480	42151550	2.05	1.35	6.74	5.00
Il1rn	20042700	60765570	3.03	8.90	40.04	4.50
Plpp3	15472890	66761900	4.31	21.82	52.04	2.39
P4ha3	14752360	43063280	2.92	38.11	81.68	2.14
Rufy3	10616410	29066600	2.74	4.39	8.82	2.01
Rrm2	8757544	37681400	4.30	13.09	37.48	2.86
Lgals9	7630653	17574580	2.30	4.41	11.09	2.52
Top2a	5817056	12842100	2.21	8.98	19.58	2.18
Ttyh3	5485562	35086060	6.40	10.46	21.88	2.09
Timp1	5446187	13657780	2.51	621.13	1797.41	2.89
Mt2	5337880	11282930	2.11	1470.42	7069.73	4.81
Sorl1	5273122	15998130	3.03	5.00	10.23	2.04
Vcam1	5265081	33679840	6.40	7.73	24.00	3.11
Xdh	5139618	17784530	3.46	0.54	4.17	7.71
Atp1b1	4760890	20713530	4.35	0.37	6.54	17.62
Cyp1b1	4467622	24652690	5.52	32.66	109.35	3.35
Tinagl1	4294986	8662477	2.02	15.15	49.53	3.27
Nid1	4017366	9807333	2.44	2.83	6.57	2.32
Eng	3920848	19044830	4.86	3.49	7.33	2.10
Cxcl12	3743041	82994030	22.17	389.90	2831.06	7.26
Clu	3581137	24472920	6.83	122.16	321.40	2.63
Prss23	3410412	23391200	6.86	33.51	71.82	2.14
Ppif	3340422	16465260	4.93	3.68	13.91	3.77
Myoc	3077883	19585150	6.36	17.54	86.38	4.93
Hs6st2	3016240	28088240	9.31	42.12	119.35	2.83
Tjp2	2679283	6709965	2.50	1.44	4.74	3.30

(Continue…)

Table. S5

	Mass Spectrometry (Identified Peptide Count)			RNA-seq (TPM)		
Gene name	**Cont**	**Cart-miR-23 KO**	**Fold Change**	**Cont**	**Cart-miR-23 KO**	**Fold Change**
Crlf1	2508715	18624450	7.42	8.73	43.59	4.99
Anln	2236792	5140888	2.30	2.29	4.81	2.10
Lpl	2222832	15952490	7.18	78.62	158.78	2.02
Ccn3	2150312	14033260	6.53	9.01	56.57	6.28
Ephb6	2130838	6526919	3.06	6.36	17.09	2.69
Tdrp	2066204	4313554	2.09	0.78	3.42	4.40
Pm20d1	1981226	7933452	4.00	0.28	0.76	2.75
Il3ra	1862561	4298940	2.31	1.19	2.61	2.20
Mgst1	1576546	4471263	2.84	4.10	10.84	2.64
Fabp7	1540417	4058362	2.63	1.19	3.93	3.30
Gba2	1414731	4404064	3.11	1.08	2.68	2.48
Nes	1177270	10239480	8.70	0.73	2.41	3.30
Postn	1162173	4845063	4.17	3.07	8.10	2.64
Lpin1	1133115	2668860	2.36	9.38	22.18	2.37
Ccdc126	1089689	2845145	2.61	2.44	5.38	2.20
Me3	1084754	2434075	2.24	0.65	1.66	2.57
Prg4	1061632	3226544	3.04	65.32	140.99	2.16
Dlk1	990338	9978799	10.08	25.79	347.08	13.46
Ggt5	948152	5120349	5.40	2.33	6.60	2.83
Kif1a	939535	6737272	7.17	0.93	2.18	2.34
Mustn1	868357	20732120	23.88	3.87	34.11	8.81
Gbp2	867185	5713468	6.59	0.38	2.51	6.61
Mki67	846723	1722916	2.03	0.95	2.09	2.20
Hmmr	796488	2638066	3.31	2.46	8.66	3.52
Spc24	726270	1658242	2.28	4.90	12.34	2.52
Ltbp2	687049	5748239	8.37	0.85	11.37	13.40
Zwint	639869	4229712	6.61	30.27	156.87	5.18
Nek6	585576	2256154	3.85	4.72	12.84	2.72
Parvb	440050	1648774	3.75	0.76	1.67	2.20
Coq5	412104	1030297	2.50	6.11	14.49	2.37
Grem1	397151	3486111	8.78	1.85	6.35	3.44
Tpx2	341218	2428677	7.12	5.50	14.22	2.59
Fhit	336059	736413	2.19	3.34	7.35	2.20
Ube2c	327086	804840	2.46	29.70	82.83	2.79
Sncg	282876	1942897	6.87	1.12	13.61	12.11
Rab3b	275670	989514	3.59	0.58	1.58	2.75
Kif20a	229068	1139925	4.98	1.83	10.05	5.51
Wdfy1	224811	10656230	47.40	2.10	19.22	9.14
Pyroxd2	203128	1065998	5.25	1.53	4.37	2.86
Igfbp2	168292	1435285	8.53	5.86	17.74	3.03
Tmod1	139475	1196372	8.58	0.91	3.00	3.30
Prc1	125860	636219	5.05	12.02	32.39	2.69
Erbb2	83480	183644	2.20	1.34	3.15	2.36
Plau	65157	1603249	24.61	0.82	2.25	2.75
Ttyh2	25759	181938	7.06	7.69	15.72	2.04
Msr1	24735	60913	2.46	6.72	17.02	2.53

Table. S6

No.	Gene Symbol	Ensembl ID	Predicted target* of			
			miR-23-3p	miR-27-3p	miR-24-3p	miR-140-5p
1	RAP1B	ENST00000250559.9	✓	✓	✓	✓
2	NCOA1	ENST00000405141.1	✓	✓	✓	✓
3	STRN	ENST00000263918.4	✓	✓	✓	✓
4	DTNA	ENST00000283365.9	✓	✓	✓	✓
5	CELF2	ENST00000379261.4	✓	✓	✓	✓
6	NLK	ENST00000407008.3	✓	✓	✓	✓
7	CTCF	ENST00000264010.4	✓	✓		✓
8	YES1	ENST00000577961.1	✓	✓		✓
9	RAP2B	ENST00000323534.2	✓	✓		✓
10	ABCA1	ENST00000374736.3	✓	✓		✓
11	PPP1R12A	ENST00000261207.5	✓	✓		✓
12	PAX9	ENST00000361487.6	✓	✓		✓
13	WDR37	ENST00000358220.1	✓	✓		✓
14	ADAMTS5	ENST00000284987.5	✓	✓		✓
15	FOXP2	ENST00000408937.3	✓	✓		✓
16	LPHN2	ENST00000370715.1	✓	✓		✓
17	PARD6B	ENST00000371610.2	✓	✓		✓
18	BAZ2B	ENST00000392782.1	✓	✓		✓
19	BMP2K	ENST00000335016.5	✓	✓		✓
20	MFHAS1	ENST00000276282.6	✓	✓		✓
21	ZHX1	ENST00000395571.3	✓	✓		✓
22	SATB2	ENST00000417098.1	✓	✓		✓
23	ANKFY1	ENST00000341657.4	✓	✓		✓
24	JHDM1D	ENST00000397560.2	✓	✓		✓
25	CELF1	ENST00000395290.2	✓	✓		✓
26	TEAD1	ENST00000361905.4	✓	✓		✓
27	PRR14L	ENST00000434485.1	✓	✓		✓
28	WEE1	ENST00000299613.6	✓	✓		✓
29	STOX2	ENST00000308497.4	✓	✓		✓
30	MARK1	ENST00000366918.4	✓	✓		✓
31	TRIM44	ENST00000299413.5	✓	✓		✓
32	APPBP2	ENST00000083182.3	✓	✓		✓
33	VCPIP1	ENST00000310421.4	✓		✓	✓
34	NDST1	ENST00000261797.6	✓		✓	✓
35	B3GNT1	ENST00000311181.4	✓		✓	✓
36	YOD1	ENST00000315927.4	✓		✓	✓
37	SNX27	ENST00000368843.3	✓		✓	✓
38	SYS1	ENST00000243918.5	✓		✓	✓
39	LHFPL2	ENST00000515007.2	✓		✓	✓
40	FAM175B	ENST00000298492.5	✓		✓	✓
41	PURB	ENST00000395699.2	✓		✓	✓
42	FAM46A	ENST00000369754.3	✓		✓	✓
43	ANKRD52	ENST00000267116.7	✓		✓	✓
44	CCDC85C	ENST00000380243.4		✓	✓	✓
45	HEG1	ENST00000311127.4		✓	✓	✓
46	TSC22D2	ENST00000361875.3		✓	✓	✓
47	PDGFRA	ENST00000257290.5		✓	✓	✓
48	ROR1	ENST00000371079.1		✓	✓	✓
49	ZBTB20	ENST00000462705.1		✓	✓	✓
50	MED13	ENST00000397786.2		✓	✓	✓
51	RAD54L2	ENST00000409535.2		✓	✓	✓
52	RC3H1	ENST00000367696.2		✓	✓	✓
53	ERC2	ENST00000288221.6		✓	✓	✓
54	NFAT5	ENST00000354436.2		✓	✓	✓
55	AP2B1	ENST00000262325.7		✓	✓	✓

*Source: TargetScan 8.0 https://www.targetscan.org/vert_80/